Global and Planetary Change 192 (2020) 103224

Contents lists available at ScienceDirect

Global and Planetary Change

journal homepage: www.elsevier.com/locate/gloplacha

From Khersonian drying to Pontian "flooding": late Miocene stratigraphy and palaeoenvironmental evolution of the Dacian Basin (Eastern Paratethys)

S. Lazarev[a,*], A. de Leeuw[b,c], M. Stoica[d], O. Mandic[e], C.G.C. van Baak[a,b], I. Vasiliev[f], W. Krijgsman[a]

[a] Paleomagnetic Laboratory «Fort Hoofddijk», Department of Earth Sciences, Utrecht University, Budapestlaan 17, 3584 CD Utrecht, the Netherlands
[b] CASP, West Building, Madingley Rise, Madingley Road, CB3 0UD Cambridge, United Kingdom
[c] Institut des Sciences de la Terre (ISTerre), Université Grenoble Alpes, CS40700, 38058 Grenoble, France
[d] Department of Geology, University of Bucharest, Bălcescu Bd. 1, 010041 Bucharest, Romania
[e] Geological-Palaeontological Department, Natural History Museum Vienna, Burgring 7, 1010 Vienna, Austria
[f] Senckenberg Biodiversity and Climate Research Centre, Senckenberganlage 25, 60325 Frankfurt am Main, Germany

ARTICLE INFO

Keywords:
Eastern Paratethys
Dacian basin
Maeotian
Khersonian
Invertebrate fauna
Palaeoenvironmental evolution
Sedimentology

ABSTRACT

In the late Miocene, a large inland sea known as the Eastern Paratethys stretched out across the present-day Black Sea – Caspian Sea region. The basin was mostly endorheic and its water budget thus strongly dependent on regional climate. The basin was therefore prone to high-amplitude water-level fluctuations and associated turnovers in water chemistry and fauna. Profound palaeoenvironmental changes happened in the Eastern Paratethys during this time period. This article documents the evolution of the Dacian Basin of Romania, the westernmost branch of the Eastern Paratethys, during the time interval between 7.7 and 6.0 Ma. Our integrated study of sedimentary facies, micro- and macro fauna along the Slănicul de Buzău Section was constrained with a timeframe based on magnetostratigraphy. The remarkable 1.3 km-thick sedimentary record, high depositional rate (0.65–1.26 m/kyr) and abundance of fossils along this section provide a unique opportunity to study sedimentary and biotic turnovers in high detail. Our analyses reveal several marked water-level and salinity changes: A predominance of freshwater coastal plain environments, only occasionally flooded, indicates a low water-level in the Khersonian (~7.7–7.63 Ma). The coastal plain deposits are overlain by offshore muds revealing a low mesohaline early Maeotian transgression, which was followed by the installation of littoral/nearshore environments with freshwater molluscs in shallow settings and oligohaline ostracods in slightly deeper settings. Subsequent delta progradation and a prevalence of freshwater fauna in both marginal and more distal environments characterize the late Maeotian. This was followed by a remarkable freshwater transgression that started at 6.3 Ma and led to predominantly offshore deposition. The late Maeotian fossil record suggests brackish water pulses from Lake Pannon (Central Paratethys), followed by mass occurrences of *Coelogonia novorossica*. At 6.1 Ma, a short influx of meso- to polyhaline microfauna including benthic and planktonic foraminifera defines the "Pontian Salinity Incursion". Molluscs, including *Eupatorina littoralis*, that biostratigraphically mark the onset of the Pontian arrived with a negligible delay of ~5 kyr after the microfauna influx. The onset of the Pontian at Slănicul de Buzau at 6.1 Ma (± 5 kyr), is thus synchronous with the onset in other Paratethys basins. Our integrated approach, placing the preserved fossil fauna in its respective sedimentary environment, allows for a detailed insight into the salinity of coeval marginal as well as basinal environments and could be more widely applied in the Paratethys realm and other semi-isolated basins with a deviant salinity.

1. Introduction

Plate tectonic collision processes generally cause uplift of extensively elongated mountain ranges, which can transform marginal epicontinental seas into semi-isolated basins. These basins may become completely isolated brackish water lakes (Rögl, 1999; Popov et al., 2006), sometimes with ephemeral connections to the open ocean (Palcu et al., 2019a; Simon et al., 2019), and their palaeoenvironmental evolution and sedimentological architecture are different from normal marine basins (Stoica et al., 2013; Jorissen et al., 2019). The

* Corresponding author.
E-mail address: s.lazarev@uu.nl (S. Lazarev).

https://doi.org/10.1016/j.gloplacha.2020.103224
Received 24 July 2019; Received in revised form 18 May 2020; Accepted 19 May 2020
Available online 28 May 2020

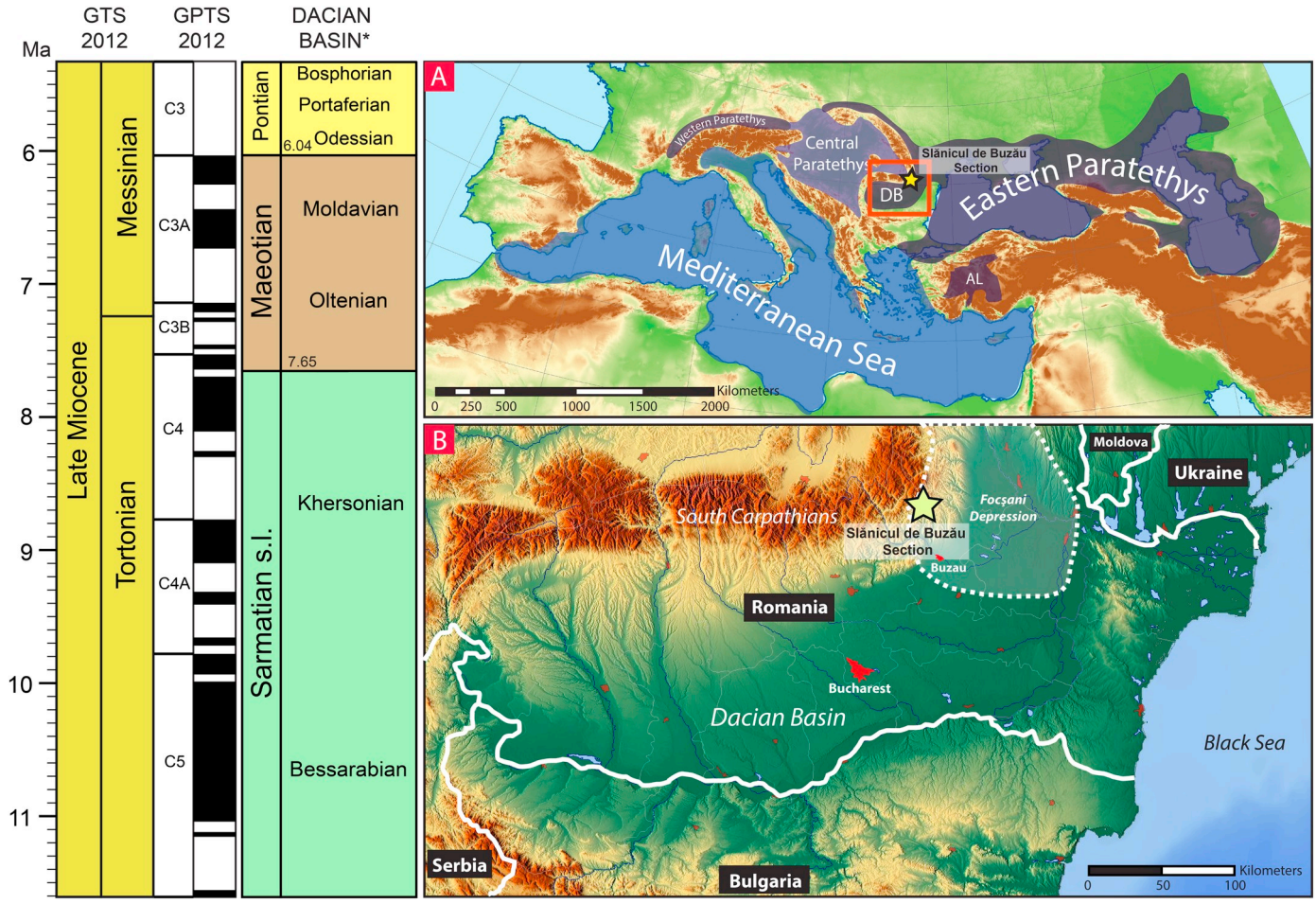

Fig. 1. Location map of the Slănicul de Buzău section and time scale. Columns from left to right: Global time scale (GTS) and Geomagnetic polarity time scale (GPTS) (Hilgen et al., 2012) and the Dacian Basin regional stages. The age constraints for the regional stage boundaries: the Khersonian–Maeotian boundary – 7.65 Ma (Palcu et al., 2019b), the Maeotian–Pontian boundary – 6.04 Ma (Krijgsman et al., 2010; Stoica et al., 2013). Position of the section in relation to: A. Paratethys; B. Dacian Basin. Abbreviations: DB – Dacian Basin, AL – Anatolian lakes. The present-day Dacian Basin (the map base is taken from www.maps-for-free.com).

Oligocene–Miocene Paratethys Sea of Central Eurasia, and its present-day remnants the Black Sea and Caspian Sea, are archetypes of such semi-isolated basins. During the Miocene, tectonic uplift of the Alpine-Carpathian-Dinaride-Pontides-Caucasus mountains isolated the Paratethys from the Tethys ocean and separated this ancient sea into several long-lived anomalohaline lake systems in the Pannonian, Dacian, Euxinian and Caspian basins (Popov et al., 2006). In these anomalohaline water masses, the faunal response to tectonically and climatically induced base-level variations, and the related changes in depositional environment, are still poorly understood and require detailed integrated studies.

The Miocene evolution of the Paratethys region (Fig. 1A) has become a major research focus over the last decades. In particular, the link between events in the Paratethys and the stepwise evolution of the Messinian Salinity Crisis in the Mediterranean Sea was investigated (Vasiliev et al., 2005; Popescu, 2006; Gillet et al., 2007; Krijgsman et al., 2010; Leever et al., 2010). This spectacular late Miocene event had an enormous impact on the regional landscapes and ecosystems of the Mediterranean region (Roveri et al., 2014), but its impact on the Paratethys appeared to be relatively limited (Krijgsman et al., 2010; Stoica et al., 2013; La Vara et al., 2016; van Baak et al., 2017). It is even more likely that Paratethys exerted a strong influence over the events in the Mediterranean through its fresh(er) water outflow (Marzocchi et al., 2016; Stoica et al., 2016; Grothe et al., 2018; Grothe et al., 2020).

In contrast, profound sea-level changes and associated turnovers in water chemistry and faunal associations took place in Paratethys during the late Tortonian–early Messinian (Khersonian–Maeotian) (Kojumdgieva et al., 1989; Popov et al., 2010; Palcu et al., 2019b). Prominent unconformities exist in the Dacian Basin (Palcu et al., 2019b) and on the coast, shelf and in the deepwater of the Black Sea (Tari et al., 2015; Golovina et al., 2019) and require a shift of attention towards the Khersonian–Maeotian events.

During the late Miocene, the Dacian basin was mostly a silled embayment and a western branch of the Euxinian (Black Sea) Basin (Fig. 1) and their palaeoenvironmental evolutions were tightly linked. The Dacian Basin formed in the foreland of the Carpathians and accommodated a remarkable sedimentary record due to very high rates of late Miocene to Pliocene subsidence and deposition (0.6–1.5 m/kyr) (Matenco et al., 2003; Tărăpoancă et al., 2003; Vasiliev et al., 2004; Jipa and Olariu, 2009). Foreland propagation of thrusting in the Quaternary uplifted part of the late Miocene to Pliocene foreland basin infill, generating excellent exposures in the SE Carpathians that enable high resolution palaeoenvironmental reconstructions.

In this paper, we focus on the late Tortonian–early Messinian (Khersonian–Maeotian) interval in the Dacian Basin, in particular on the Slănicul de Buzău section. We integrate sedimentary facies analyses with palaeoecological information from molluscs and microfauna, and provide palaeomagnetic age constraints. The main aim is to document the palaeoenvironmental changes occurring in the Dacian Basin between the Khersonian (Tortonian) and Pontian (Messinian) Paratethyan base-level changes.

The Slănicul de Buzău section is located in the Romanian southeast

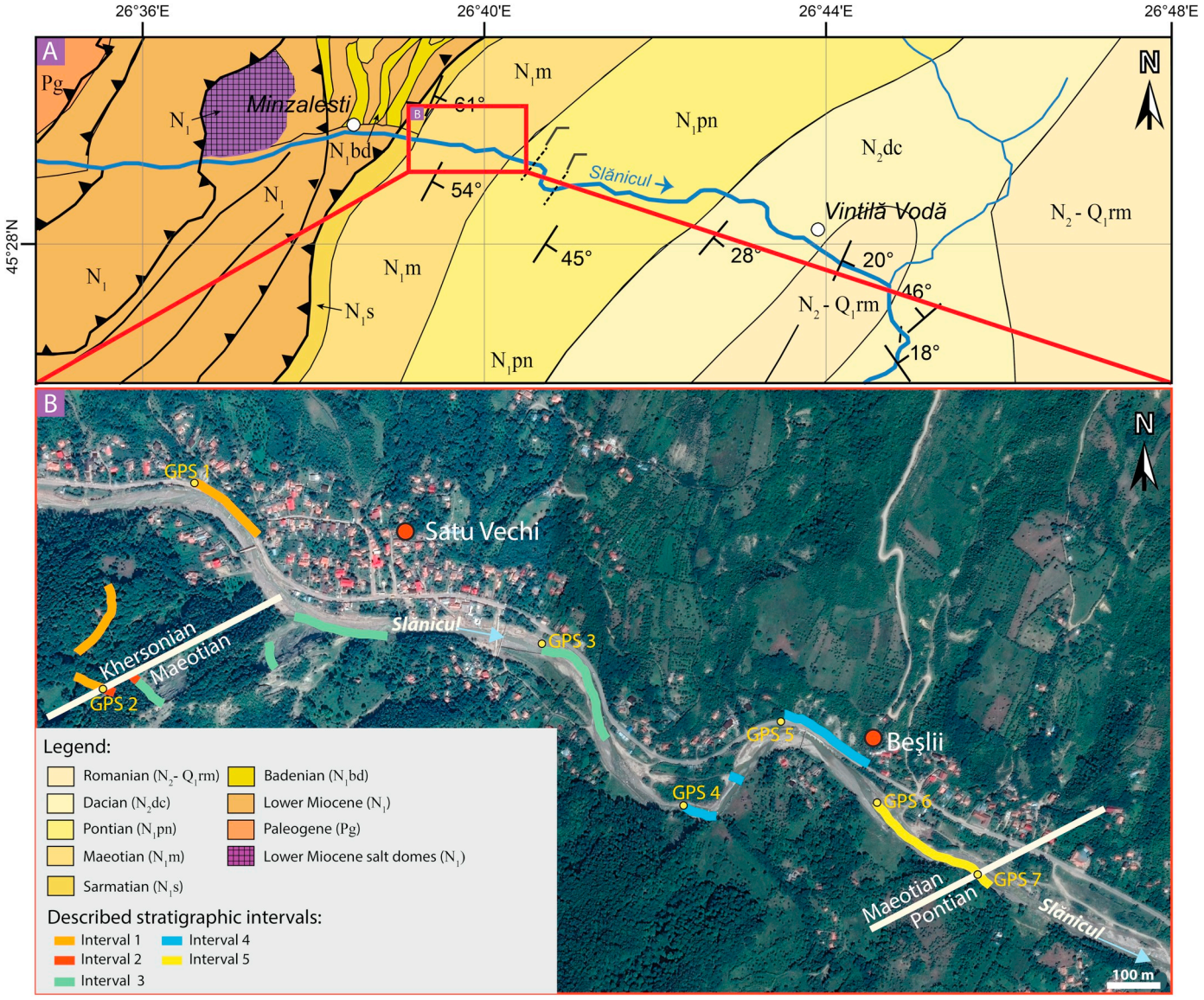

Fig. 2. Geological setting of the studied section. A. Geological map (Motas et al., 1966; Dumitrescu et al., 1970); B. Position of the studied stratigraphic intervals in the Slănicul de Buzău area. The aerial photo image credit: Google Earth.

Carpathians near the Focşani Depression – one of the main depocentres in the Carpathian foreland (Fig. 1B and 2). It represents the thickest and best-exposed succession of Miocene to Pleistocene sediments in the Dacian Basin (Motas et al., 1966; Dumitrescu et al., 1970) that was the subject of several earlier studies, e.g. with a focus on general palaeogeographic characteristics (Jipa and Olariu, 2009), regional geodynamic evolution (Dupont-Nivet et al., 2005; Vasiliev et al., 2009), and palaeoenvironmental changes in the Pontian (Snel et al., 2006; Grothe, 2016), Dacian (Jorissen et al., 2018) and Romanian (van Baak et al., 2015). However, the palaeoenvironmental evolution during the Khersonian–Maeotian was poorly investigated.

2. Geological setting

2.1. The Dacian Basin as a part of the Eastern Paratethys

The Dacian Basin is a foreland basin that formed in the middle Miocene at the foot of the Eastern and Southern Carpathians (Fig. 1b). It was part of the Paratethys Sea (Matenco et al., 2003; Jipa and Olariu, 2009; ter Borgh et al., 2014), which was a Eurasian sea that extended from the Alps in the West to the Aral Sea in the East (Laskarev, 1924; Rögl, 1999; Schulz et al., 2005) (Fig. 1A).

After the Eocene–Oligocene, Paratethys was constantly shrinking in size (Rögl, 1999; Schulz et al., 2005). In the late Miocene, the formation of the Carpathian arcuate belt invoked a final separation of the Paratethys into two parts – the Eastern Paratethys (Euxinian, Caspian and Dacian Basins) and the Central Paratethys (Pannon Lake) (Tărăpoancă et al., 2003; Schmid et al., 2008; Vasiliev et al., 2010; ter Borgh et al., 2013; ter Borgh et al., 2014).

The evolution of these Paratethys basins was inextricably determined by their numerous sea-level variations caused by an intricate interplay between climate fluctuations and tectonics (De Leeuw et al., 2010; Leever et al., 2010; Popov et al., 2010; Palcu et al., 2015; De Leeuw et al., 2018; Palcu et al., 2019b; Simon et al., 2019). Consequently, connections between basins opened and closed repeatedly. Base level, salinity and implicitly fauna and ecosystems were strongly controlled by a delicate balance between precipitation and evaporation as well as by the dynamics of the gateways to the open ocean (Leever et al., 2010; Karami et al., 2011; Vasiliev et al., 2015; Simon et al., 2019). Any disturbances in these parameters caused marked palaeoenvironmental responses (Palcu et al., 2015; Mandic et al., 2019).

In its evolution, the Dacian Basin went through three main stages: 1)

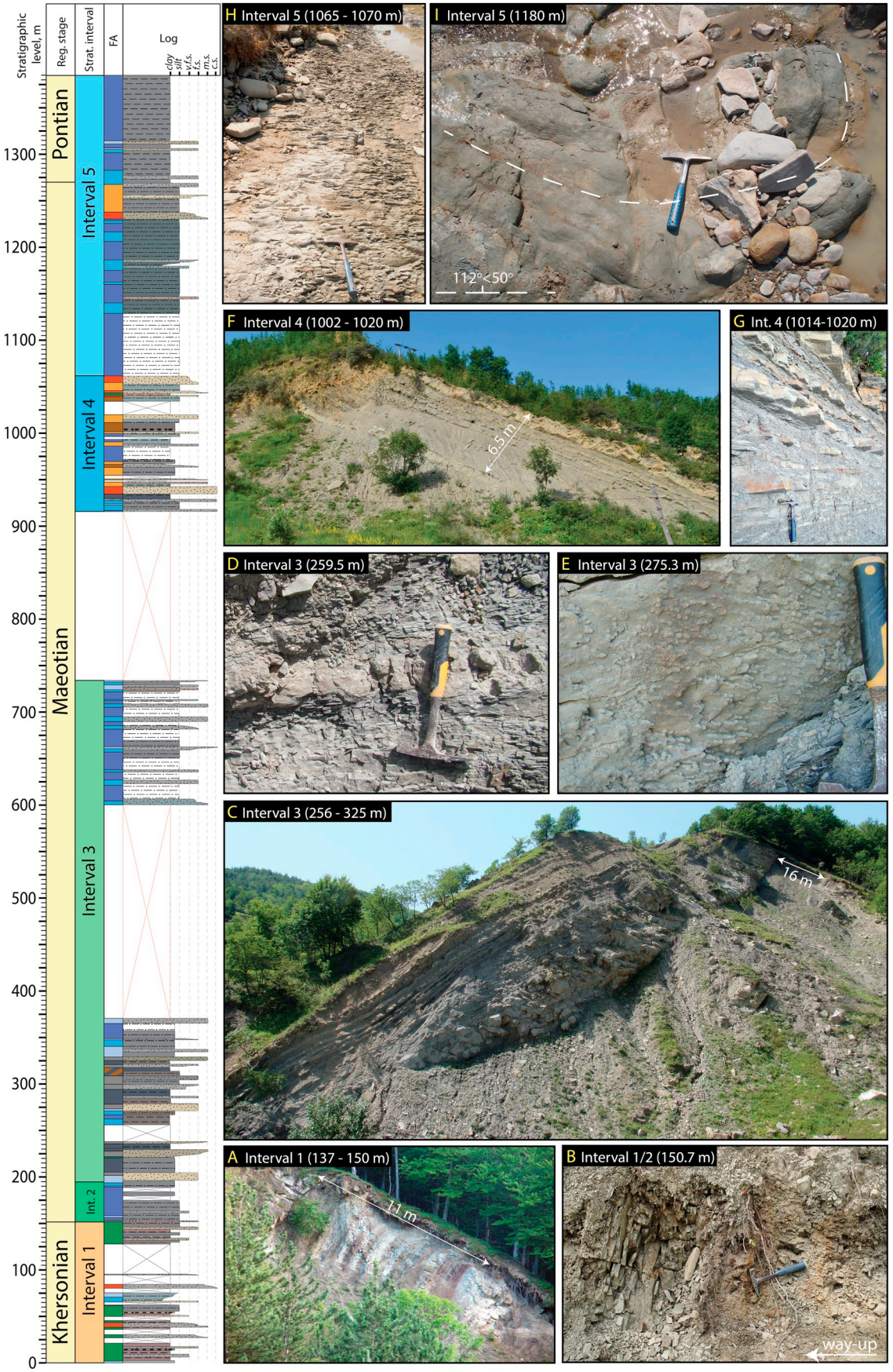

(caption on next page)

Fig. 3. General log of the upper Khersonian–Maeotian–lowermost Pontian interval of the Slănicul de Buzău section. Green arrows – mollusc samples, blue arrows – microfauna samples. A. Floodplain, continental environments of Stratigraphic Interval 1 (SI1); B. Khersonian–Maeotian Boundary. Khersonian red palaeosoils are covered by Maeotian fissile siltstones. Top to the left.; C. Thick barrier island sandstone body followed by thin washover sandstones (SI3); D. Storm layer occurring in the offshore transition environment with chaotically distributed shells of *Viviparus moldavicus* (mollusc sample 99); E. Traces of *Diplocraterion* on the base surface of the barrier island sandstone (SI 3); F. Shallowing-upwards succession of deltaic deposits (SI 4); G. Alternation of current-ripple cross-laminated sandstone and mudstone in delta front environment (SI 4); H. Offshore thinly-laminated clays of SI 5; I. Slump within the offshore clays of the SI 5. The colour meaning in the facies association column is shown in the legend of Fig. 4. (For interpretation of the references to colour in this figure legend, the reader is referred to the web version of this article.)

The late middle Miocene–mid late Miocene interval with brackish to polyhaline water environments and the widest connectivity with the Euxinian (Black Sea) Basin (Palcu et al., 2017); 2) The mid late Miocene–mid Pliocene interval with changing salinity from brackish to freshwater and restricted connectivity with the Euxinian Basin (Stoica et al., 2013); 3) The mid Pliocene–Pleistocene interval, in which the basin became overfilled and accumulated fluvial and limnic deposits (Jipa and Olariu, 2009; van Baak et al., 2015; Jorissen et al., 2018; Matoshko et al., 2019).

2.2. Regional stages and chronostratigraphy

In the Black Sea and Dacian Basin region, the late Miocene regional time scale comprises the Bessarabian, Khersonian (both are parts of Sarmatian s.l.), Maeotian and Pontian regional stages (Fig. 1) (Piller et al., 2007; Hilgen et al., 2012). To clarify the time frames of our research and to avoid misunderstanding among non-regional researchers, we briefly explain the Eastern Paratethys regional stages here.

The Sarmatian stage was introduced by Suess (1866). The Sarmatian is used in both the Central and Eastern Paratethys, albeit with different durations and biostratigraphic divisions. In our study, we use a subdivision of the Sarmatian into three substages generally applied to the Eastern Paratethys: Volhynian (Lower), Bessarabian (Middle) and Khersonian (Upper). The base Sarmatian boundary (Badenian – Sarmatian) in the Dacian Basin was magnetostratigraphically dated at 12.65 Ma and correlated to chron C5Ar.1r (Palcu et al., 2015).

During the Sarmatian, the Eastern Paratethys became isolated from the open ocean with consequent gradual extinction of marine forms inherited from the Badenian (Iljina et al., 1976). The most pronounced palaeoenvironmental changes happened in the Khersonian when the Eastern Paratethys endured a series of marked water-level drops (Tugolesov et al., 1985; Popov et al., 2006; Palcu et al., 2019b). This resulted in disconnection of its various subbasins, and extinction of the last marine assemblages dominated by oligo-, mesohaline molluscs of *Chersonimactra* sp. (Iljina et al., 1976; Kojumdgieva et al., 1989; Paramonova, 1994). In the Black Sea (Euxinian Basin), the Khersonian–Maeotian boundary has been dated magnetostratigraphically (Trubikhin, 1989; Radionova et al., 2012) and cyclostratigraphically (Rybkina et al., 2015) at ~7.6 Ma (correlation to C4n.1n) and in the Dacian Basin (correlation to C4n.1r – C3Br.2r chrons) it was recently dated at 7.65 Ma (Palcu et al., 2019b).

The Maeotian stage was named by Andrusov (1890) and divided into two substages – Oltenian and Moldavian in the Dacian Basin (Wenz, 1942; Roshka, 1973; Vereshchagin, 1982). The Maeotian stage started with a marked transgression that ended the Khersonian lowstand, increased connectivity between the Euxinian, Caspian and Dacian basins, and led to the spread of brackish water biota (Popescu, 2006; Palcu et al., 2019b). In the Dacian Basin, the lower Maeotian (Oltenian) shows an alternation of molluscs tolerant to a range of different salinities: freshwater unionids and neritids (*Unio*, *Theodoxus*), freshwater to brackish water dreissenids and marine *Dosinia*, *Abra* and *Ervilla* (Wenz, 1942; Iljina et al., 1976). The upper Maeotian (Moldavian) is defined by the wide distribution of freshwater and slightly brackish water gastropods such as *Theodoxus stefanescui* and *Pontohydrobia ossovinarum*, occasionally in combination with *Andrusoviconcha modiolopsis* (Wenz, 1942; Roshka, 1973; Iljina et al., 1976). The Maeotian is followed by the **Pontian stage**, which starts slightly before the onset of the MSC in the Mediterranean (Krijgsman et al., 2010; Stoica et al., 2013). The Maeotian–Pontian boundary is characterized by a short influx of poly-, mesohaline microfauna assemblages dominated by foraminifera *Ammotium*, *Ammonia*, *Streptochilus* and *Tenuitellina*, and followed by occurrence of the lower Pontian molluscs *Paradacna*, *Eupatorina* and *Pontalmyra* (Roshka, 1973; Iljina et al., 1976; Vereshchagin, 1982; Stevanovic et al., 1989; Snel et al., 2006; Popov et al., 2016; Stoica et al., 2016).

The Maeotian–Pontian boundary has been dated cyclostratigraphically at ~6.1 Ma in the Black Sea and Caspian Sea (Chang et al., 2014; van Baak et al., 2016; Rostovtseva and Rybkina, 2017), and magneto-biostratigraphically at 6.04 Ma in the Dacian Basin (slightly below C3r–C3An.1n polarity switch) (Krijgsman et al., 2010; Stoica et al., 2013).

3. Material and methods

3.1. The Slănicul de Buzău section

The Khersonian–Pontian interval in the Slănicul de Buzău valley is located in the NW flank of a syncline (Fig. 2A) that determines a gradual flattening of the bedding plane from 112°/60° SE at the base of the section to 120°/48° SE at the top of the section. The studied interval is 1380 m thick, with 700 m being well exposed (Figs. 3, 4). The described interval begins in Khersonian deposits exposed on the left side of the Slănicul river, along the Mânzălești – Vechi road (GPS 45°29'18.74" N; 26°39'10.30"E) and ends in the Pontian deposits on the right side of the same river near Besli village (Sample SB135, GPS 45°28'58.24"N; 26°40'25.30"E). The thickness of the section including the non-exposed intervals was measured in the field and subsequently corrected using satellite maps, GPS points and bedding parameters.

3.2. Sedimentology

Sedimentological study of the Khersonian–Maeotian interval of Slănicul de Buzău is based on field observations that were focused on description of lithofacies (lithology, grain-size, colour, sedimentary structures) and associated trace fossils. The descriptive terminology followed the field guide of Tucker (2012), while the general facies concept is based on Miall (1996). Later, the commonly occurring lithofacies were combined into 9 distinct facies associations (Table 1) following the concept of Collinson (Collinson, 1969; Posamentier and Walker, 2006). The facies associations were attributed to certain depositional environments based on sedimentological reasoning and a comparison with well-known literature examples (Table 1).

3.3. Biostratigraphy

Thirty five mollusc samples with a weight of about 1 kg were first hand picked for larger specimens to prevent their fragmentation. The residues were then washed and sieved through a sieve with a 1 mm mesh size. Identifications, taxonomic classification and palaeoecological interpretations are based on (WoRMS Editorial Board, 2020; Wenz, 1942; Kojumdgieva, 1969; Stevanovic and Iljina, 1982; Stevanovic and Paramonova, 1983; Nevesskaja et al., 1993;

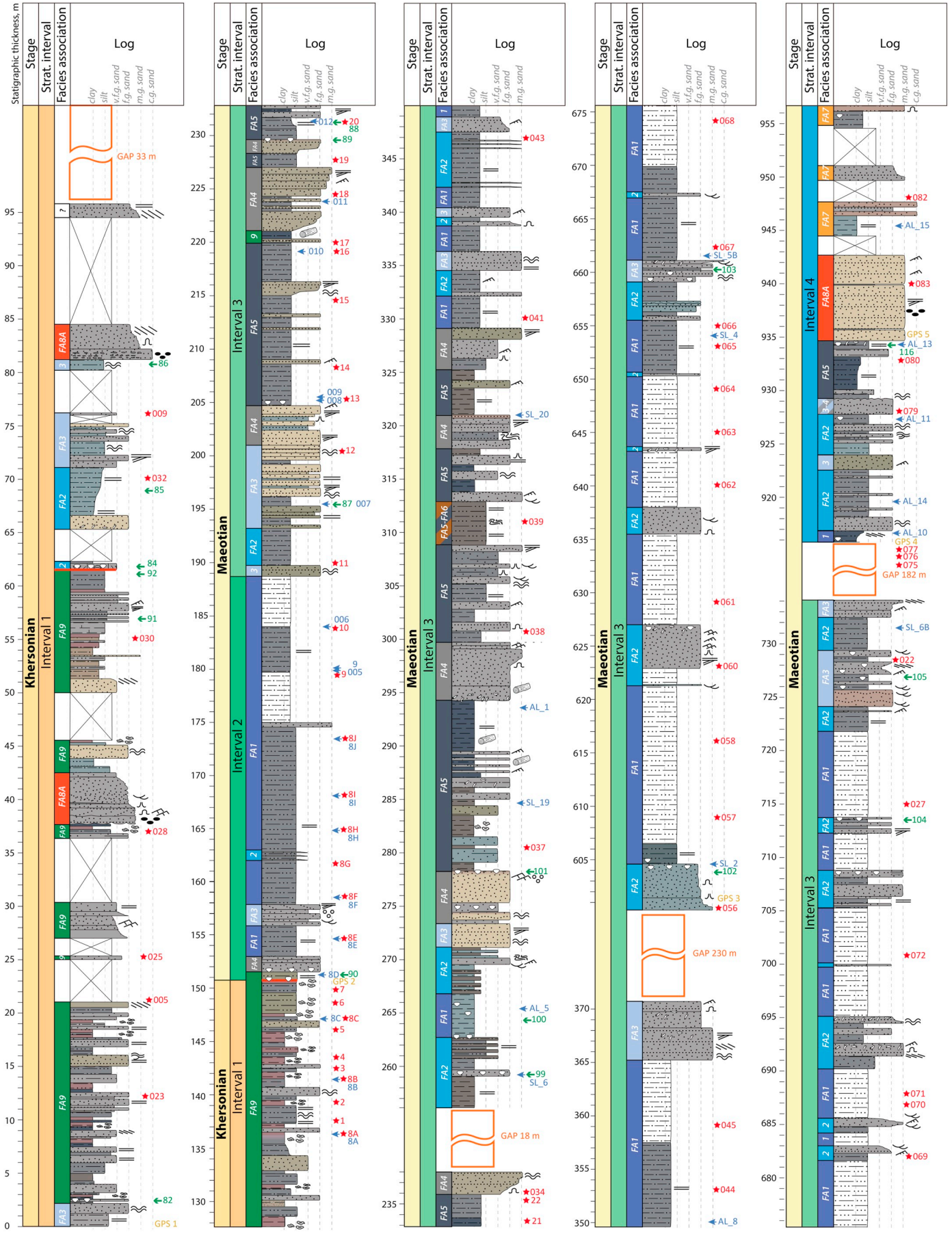

Fig. 4. (Parts 1 and 2). Detailed sedimentary log of the upper Khersonian-Maeotian-lowermost Pontian interval of the Slănicul de Buzău section with sampling points and sedimentary structures and facies associations indicated.

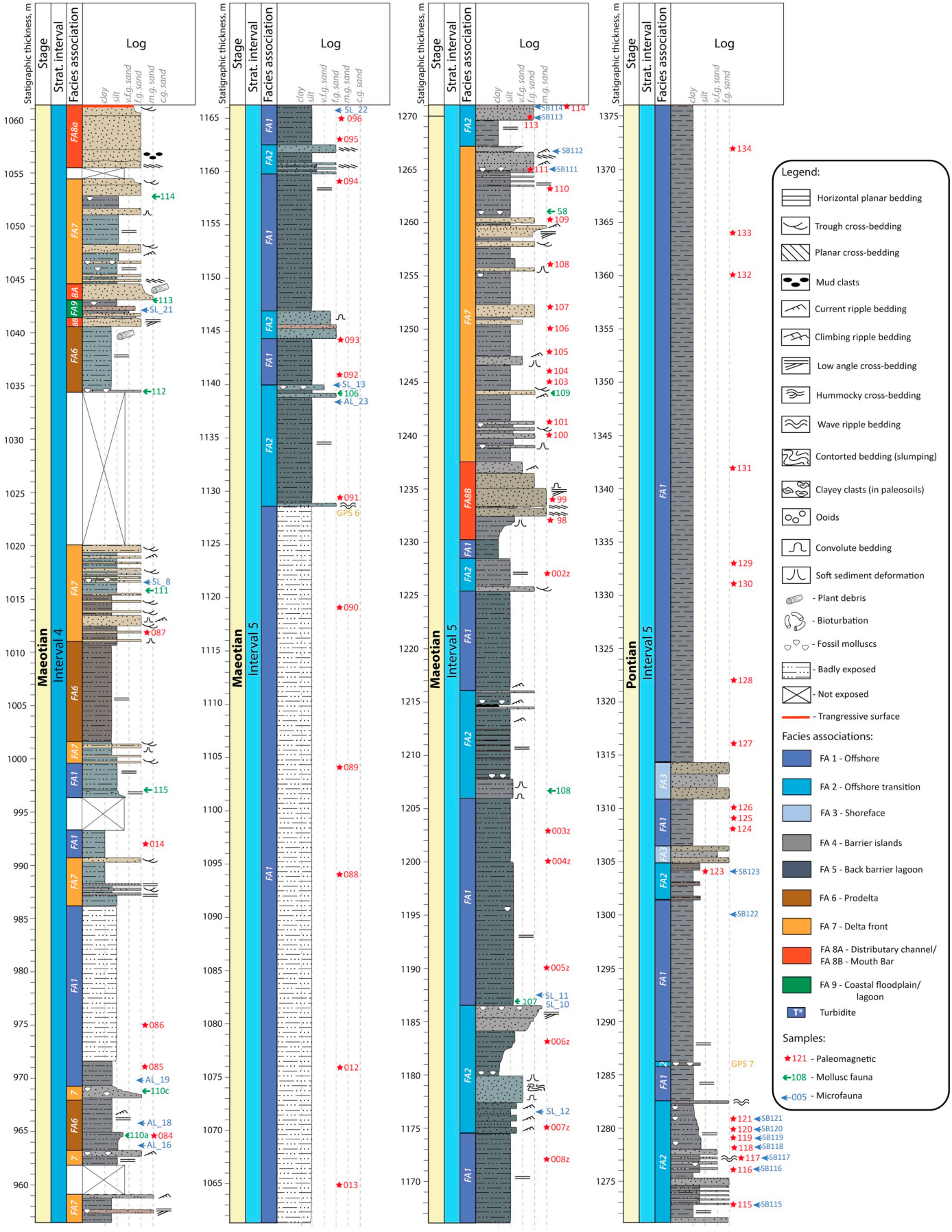

Fig. 4. (*continued*)

Table 1
Characteristics of lithological facies associations recognized in the Khersonian–Maeotian interval of the Slănicul de Buzău section.

Description	Interpretation
FA 1: Grey, bluish grey, fissile, thinly (1–2 mm) parallel-laminated claystones and siltstones, containing sporadic up to 5 cm-thick beds of grey muddy fine-grained sandstone lacking sedimentary structures. FA1 usually covers FA3 with a sharp contact. Gradually passes upwards into FA2.	**Offshore.** Relatively deep-water and low-energy offshore zone as indicated by the predominantly fine grain-size and thin lamination. Similarly interpreted facies are known from the open marine shelf in the Upper Cretaceous of the Back Tongue (Yoshida, 2000) and the Turonian Ferron Sandstone (Fielding, 2010), Utah and from the Late Quaternary deposits of the Po Delta (Amorosi et al., 2003; Amorosi et al., 2016).
FA2: Grey, thinly-laminated siltstones with interbedded sandstones. Sandstones occur as sharp-based (sporadic gutter casts) single beds (< 2 m) with low-angle cross lamination, soft-sediment deformation structures, climbing-ripple cross-lamination sometimes finished by a wavy top surface, or alternatively, occur as packages (< 2 m) of closely interbedded hummocky cross-stratified muddy sandstones. Typical ichnotraces belong to *Diplocraterion* – U-shape traces forming sets of double-spot patterns on the basal surface of sandstone beds, Bioturbation Index (BI) = 1–2. FA2 is usually underlain by FA1 and gradually passes upwards into FA3.	**Offshore transition zone** between fair-weather- and storm-wave base in line with storm-induced hummocky cross-stratification (Raaf et al., 1977; Cheel, 1978; Dott and Bourgeois, 1982). Soft-sediment deformation structures accompanied by climbing-ripple cross-lamination in single-bed sandstones point at a rapid deposition from sediment-laden unidirectional flows resulted from exceptional storm events (Ashley et al., 1982; Bhattacharya and MacEachern, 2009; Oliveira et al., 2011). Traces of *Diplocraterion* commonly belong to *Skolithos* ichnofacies, which is widely distributed in nearshore areas (MacEachern and Bann, 2008). Similarly interpreted facies occur in the Cretaceous Sego Sandstone in Utah (van Cappelle et al., 2016), are known as lower shoreface in the Neogene cores of the Eastern Venezuela Basin (Buatois et al., 2012), or as distal lower shoreface in the Star Point Sandstone in Utah (Forzoni et al., 2015).
FA3: 1–3 m-thick coarsening- and thickening-upwards packages of grey, yellowish-grey, fine- to medium-grained sandstone. The sandstone packages consist of very thinly-bedded (3–4 cm) wave-ripple cross-laminated beds that gradually thicken up into a very thick bed (< 2 m) with wave-ripple marks. Locally, some of the beds are structureless or have a faint parallel- or low-angle cross lamination. There are also some thin oolite beds. Bioturbation mostly occurs in the uppermost beds. It generally comprises elements as *Skolithos* (simple vertical straight shafts, ø < 10 mm) and *Ophiomorpha* (vertical to horizontal shafts with bioglyphs, ø ~ 40 mm) (BI = 3–4), locally with smaller scale vertical burrows in mudground, roughly attributed to *Glossifungites* (BI = 2–3, bivalve borings, polychaete burrows). FA3 is usually underlain by FA2 with gradual contact and typically succeeded by FA4, but also by FA1, FA2.	**Shoreface**. Frequent wave-ripple cross-bedding suggests deposition within the fair-weather wave-base interval. Gradual thickening and coarsening upward and presence of FA4 on top of FA3 indicate progradation. Oolites formed on shoals, tidal bars or beaches (Flügel, 2010). *Skolithos* ichnofacies (including elements *Skolithos*, *Ophiomorpha* and *Planolites*) is typical for the near-shore zone and a non-cohesive, shifting substrate (Gérard and Bromley, 2008; MacEachern and Bann, 2008). *Glossifungites* mostly occurs in fairly turbulent waters on muddy firmgrounds drilled or scraped by bivalves or worms (Seilacher, 2007). Similar deposits were distinguished as shoreface facies in the Blackhawk Fm, Utah (Yoshida, 2000), as upper shoreface deposits in the Neogene of the Eastern Venezuela basin (Buatois et al., 2012), and as middle and upper shoreface in Reading (1996) and Tamura (2012).
FA4: 1 to 6 m thick, coarsening-upwards beds of grey structureless or low-angle cross-laminated sandstone with occasional convolute structures. In the facies association order FA3 > FA4 > FA5, the FA3 to FA4 transition is gradational and coarsening upwards, while the transition from FA4 to FA5 is sharp, with a surface covered with broken and irregularly distributed shell fragments, locally mixed with ooids. In the facies association order FA5 > FA4 > FA3, FA4 has a sharp, undulating and erosive base, with frequent traces of *Diplocraterion* (BI = 3–4) (Fig. 3C, E) (Bann et al., 2004; Gérard and Bromley, 2008). Locally, this base is covered with small irregularly shaped holes (< 3 cm), which are probably relicts of mud clasts and contains some single fragments of fossilized wood. The FA4 to FA3 transition is gradual and fining up.	**Barrier island.** A longshore-prograding sandstone body, which is separated from the mainland by lagoons and marshes (McCubbin, 1982; Reading, 1996) and has wave-dominated shoreface environments on the basin side (Hampson et al., 2009; Kieft et al., 2010). Low-angle lamination formed by shore-normal oscillatory motion (McCubbin, 1982). In shallowing trends, the barrier occurs between shoreface and lagoon deposits. In deepening trends, the barrier covers lagoon deposits and passes upwards into shoreface deposits (McCubbin, 1982; Chentnik et al., 2015). Also known from the Middle Jurassic Brent Group of the northern North Sea (Went et al., 2013).
FA5: Dark-grey to black organic-rich thinly-parallel-laminated claystone (carbonaceous shale), in intervals 0.5–10 m thick, interbedded with rare thin (< 0.3 m) beds of grey fine-grained sandstone with planar cross-lamination and thin (< 0.2 m) beds of grey fissile mudstone. Wood fragments and dispersed organic material are very abundant. *Ophiomorpha* traces (BI = 2) were observed in one of the grey silty sandstones. FA5 overlies FA4 with a non-erosive but sharp contact and is overlain by FA4 with a strongly erosive contact.	**Back-barrier lagoon**, situated behind coeval spits and barriers (Hampson et al., 2009; Kieft et al., 2010; Kieft et al., 2011; Buatois et al., 2012; Chentnik et al., 2015) and strongly influenced by freshwater and terrestrial organic matter input (Allen and Johnson, 2011). Non-periodic thin sandstone beds reflect storm washover (Hayes and FitzGerald, 2013; Chentnik et al., 2015). *Ophiomorpha* suggests marine origin (McCubbin, 1982). Also known from the Mid Jurassic of the South Viking Graben (Kieft et al., 2010), mid-to-late Jurassic of the North Sea Graben rift basin (Hampson et al., 2009), Upper Cretaceous Straight Cliffs Fm, Utah (Allen and Johnson, 2011), and Late Pleistocene-Holocene of the Po Delta (Amorosi et al., 2003).
FA6a: Thinly-bedded (< 0.03 m) grey laminated siltstones with interbedded brownish-grey massive mudstones in packages up to 2 m thick. Locally, mudstones are inversely-graded, gradually passing into fine-grained structureless sandstones. The latter ones contain some shell debris and upwards, with a gradual contact develop back into mudstones. **FA6b:** Brown, bluish-grey fissile thinly-parallel-laminated to massive mudstones with rare thin (< 0,2 m) beds of fine-grained muddy sandstone with undulating laminae and soft-deformation structures in packages up to 10 m. No bioturbation was found. FA 6 (prodelta) is delimited by FA 7 (delta front) with a gradual transition or overlies FA1 (offshore) (Figs. 8, 10) also with a gradual transition.	**Prodelta.** Deposition of sandy mudstone and sandstones at times of larger outflow and suspension fallout of mud during stagnant periods (Fielding, 2010). Inverse grading in some sandstone beds may suggest hyperpycnal flows (Mulder et al., 2003; Bhattacharya and MacEachern, 2009) during waxing river discharge periods, whereas the normally-graded beds reflect waning discharge (Mulder et al., 2003). Hyperpycnal flow may also be induced by storms (Bhattacharya and MacEachern, 2009), in line with associated shell debris and soft-deformation structures. Weakly developed undulating lamination indicates a deceleration of uni-directional flow. The lack of bioturbation suggests physio-chemical stress, i.e. prodelta changes in salinity and sediment input (MacEachern et al., 2005). Similarly interpreted facies are known from the Turonian Ferron Notom Delta Complex, Utah (Zhu et al., 2012), and the Shivugak Bluffs, Alaska (van der Kolk et al., 2015).
FA7a: 10 m-thick heterolithic packages of sharply bounded beds (< 0.3 m) of brown muddy very fine-grained sandstone and brown, bluish-grey siltstones (Fig. 3G). Sandstone beds are planar parallel-laminated or trough cross-laminated with current-ripple marks. Thicker sandstone interbeds are sometimes low-angle cross-laminated and have sole structures at the basal surface. Sharp-bounded sandstone beds are locally underlain by siltstones with soft-sediment deformation structures and, in the case of amalgamated bedding, the basal sandstone beds bear pillow structures. **FA7b:** Similar to FA7a but with a thickening-upward trend in the sandstone beds resulting in a very thick (< 2 m) sandstone at the top of each succession. Structures change from low-angle cross-lamination at the bottom of the succession, through a structureless interval, to trough and current-ripple cross-lamination in the upper part.	**Delta front.** Intervals with interbedded sandstones and mudstones reflect the distal delta front, whereas thick sandstones reflect the proximal delta front. Granulometry is strongly dependent on river discharge intensity. Coarser sand beds reflect heavily sediment- loaded outflow events, while mudstones indicate more stagnant periods (Fielding, 2010). Parallel lamination, planar cross-lamination and trough cross-lamination formed in the upper flow regime (Miall, 1996). Low-angle cross-lamination with current-ripple marks on bed tops demonstrates sand deposition in the lower flow regime. Infrequent massive sandstone beds with well-expressed soft-sediment deformation resulted from gravity flows (Oliveira et al., 2009), but the lack of gradation and structures precludes the distinction between hyperpycnal flows or turbidity currents. The

(*continued on next page*)

Table 1 (*continued*)

Description	Interpretation
Mudstones below sandstones contain marked water-escape structures. Bioturbation is not clear (BI = 0–1). FA7 is typically underlain by FA6 with a transitional coarsening-upwards contact and may be overlain either by FA6 with a transitional fining-upwards contact or erosively by FA8.	lack of bioturbation is likely linked to fluctuations in salinity, in analogy with the above-described prodelta facies. Similarly interpreted sediments are known from the Turonian Ferron Notom Delta Complex, Utah (Zhu et al., 2012) and the Shivugak Bluffs, Alaska (van der Kolk et al., 2015).
FA8A: Erosionally-based, fining-upwards, medium- to fine-grained sandstone bodies up to 8 m thick, consisting of 2–3 beds of 1–4 m thick that are amalgamated or separated by thin (< 0.01 m) layers of grey mudstone. Sandstones have an undulated basal surface (< 2 m wavelength, and < 0.4 m amplitude) with flow marks overlain by a breccia with rounded siltstone clasts up to 0.3 m in diameter. In the middle part, planar cross-lamination and some climbing ripples and mud drapes occur, while higher up there is large-scale sigmoidal, low-angle lamination, fading upwards and passing into thin planar cross-laminated sets with current ripples. There are fossilized wood fragments and plant debris, but no bioturbation. **FA8B:** Similar to FA8A except for its base, which is conformable. The lower part of the sandstone body sometimes coarsens upwards. FA 8 overlies FA7 or FA5 with erosive contact. FA8 is covered by FA7 and FA6 with a gradual fining-upwards contact, by FA9 with a gradual contact or by FA1 with a sharp contact.	**Deltaic mouth bars (8B) and distributary channels (8A)** with progressively diminishing flow. Intraformational breccia as a result of bank collapse is a typical sign of highly-erosive distributary channels (Fielding, 2010; Buatois et al., 2012; Matoshko et al., 2016). The presence of plant debris and fragments of fossilized wood are the effect of erosive reworking of the floodplain. Thin interbedded mudstones likely point at an episodic cessation of the water flow during temporary channel abandonment (Fielding, 2010). Similarly interpreted facies are known from the Eocene Hecho Group of the South-central Pyrenean foreland basin (Cronin et al., 1998) and the Turonian Ferron Sandstone (Fielding, 2010).
FA9: Packages of up to 10 m thick consisting of an alternation of reddish-brown, mottled, aggregate claystone in beds of 0.3–1 m and light-grey, yellowish-grey, structureless, locally fissile, marly mudstones and siltstones in beds of 0.2–0.4 m. Some of these mudstones contain *Ammonia beccarii* foraminifera. Occasionally, there are single beds of planar cross-laminated and current-ripple cross-laminated sandstones, 0.2–1 m thick, which exclusively overlie grey mudstones. Where reddish mottled claystone beds overlie grey mudstone beds, the contact is irregular. In a single case, a 0.5 m-thick bed of bioclastic limestone built of *Sarmatimactra* shells was observed. Bioturbation is mostly absent or obscure, but rare rootlets and rhizoliths occur. FA9 is associated with FA3 and FA8.	**Coastal plain.** Grey mudstones formed due to suspension fallout from stagnant water on the floodplain while the ones containing foraminifera accumulated during periodic small scale transgressions on the coastal plain. The red mottled claystones on top suggest subaerial exposure and are interpreted as palaeosols (Nadon and Issler, 1997; Kraus, 1999; Scherer et al., 2015). Sandstone beds are interpreted as crevasse splays filling floodplain ponds. Similarly interpreted facies are known from the Surakhany Suite, South Caspian Basin (Vincent et al., 2010), the Tertiary Duchesne River Fm, Uinta Basin (Sato et al., 2018), the Aptian Barbalha Fm, Araripe Basin (Scherer et al., 2015) and Middle Moscovian of the Kladno-Rakovník Basin (Opluštil et al., 2015).

Paramonova, 1994; Nevesskaja et al., 1997; Nevesskaya et al., 2013). For investigation of microfauna, forty five samples were washed and sieved through a sieve with 63 μm mesh size following a standard micropalaeontological approach (Stoica et al., 2013). Preparation, identification and photographing of the mollusc fauna was performed at the Natural History Museum (Vienna, Austria), while the microfauna has been processed at the University of Bucharest (Romania) (Supplementary 1).

3.4. Magnetostratigraphy

Palaeomagnetic measurements were performed in the Paleomagnetic laboratory "Fort Hoofddijk", Utrecht University, the Netherlands. For palaeomagnetic investigations, 139 stratigraphic levels were sampled with a portable drilling machine equipped with a diamond crone, water pump and a petrol generator as power supply. From each level, two standard oriented cylindrical samples were taken. A local declination correction of 5° (www.ngdc.noaa.gov) was added to all measurements to compensate for secular variation. In order to retrieve the Characteristic Remanent Magnetization (ChRM), 60 samples were demagnetized thermally (TH), 61 samples in alternating field (AF) and for 18 samples both techniques were applied. During thermal demagnetization, samples were stepwise heated with increments of 30–40 °C up to 680 °C, or to a lower temperature if the remanent magnetization became lower than 10% of its initial value. After each temperature step, samples were measured in multiple positions on a horizontal 2G Enterprise DC SQUID cryogenic magnetometer (noise level 3×10^{-12} Am^2). Measurements in alternating field (AF) were performed on a robotized handler controller attached to a horizontal 2G Enterprise DC SQUID cryogenic magnetometer (Mullender et al., 2016). Samples were gradually demagnetized in alternating field (AF) from 0 to 100 mT with increments of 2–20 mT. In addition, to determine magnetic carriers, thermomagnetic properties in air of 3 samples were measured on a horizontal-type Curie balance (noise level $5 \times 10^{-9} Am^2$) (Mullender et al., 1993). The measured magnetic directions were interpreted using the online platform Paleomagnetism.org (Koymans et al., 2016). All interpreted data are included in the manuscript (Supplementary 2-4) and can be uploaded to Paleomagnetism.org. For correlation of the acquired polarity pattern we used the Global Polarity Time Scale (GPTS) (Hilgen et al., 2012).

4. Results

4.1. Stratigraphic intervals and associated fauna

The Khersonian to lowermost Pontian sedimentary record of the Slănicul de Buzău section is highly variable. Nine facies associations (FA) were recognized (Table 1; Fig. 4). The section was moreover divided into five stratigraphic intervals (SI) (Fig. 3), for which the sedimentary facies associations, microfauna and mollusc fauna are discussed below. A discussion per stratigraphic interval was preferred over a discussion per depositional unit, because it facilitates comparison with other contemporaneous Paratethys records.

4.1.1. Stratigraphic interval 1 – upper Khersonian

Stratigraphic interval 1 consists of three lithologically distinct subintervals. The lower (0–61.2 m) and upper (127.5–150.8 m) subintervals display sandstone - grey mudstone - red claystone alternations characteristic for FA9 (Figs. 3A, 4, Table 1). The middle subinterval (61.2–127.5 m) is more poorly exposed and consists of bioclastic limestones, claystones and sandstones attributed to FA2, FA3 and FA8 (Fig. 4; Table 1).

The mollusc fauna, collected in the lower and middle parts of SI1 is dominated by *Chersonimactra caspia* and locally also contains *Coelogonia*? sp. and/or *Potamides*? cf. (Fig. 5, Table 2). At 56 m, a specimen of *Helix mrazeci* has been found (Fig. 5, Table 2). The upper part of SI1 contains no molluscs.

The microfauna of SI1 has been studied only in its upper part (Fig. 6, 127.5–150.8 m), where there is a link between fauna and lithofacies: The grey mudstones contain abundant *Ammonia beccarii* benthic foraminifera, while the red and brownish claystones either have no fossils, or contain oogonides of freshwater algae *Nitellopsis* sp., possibly *Nitellopsis meriani* (Fig. 7).

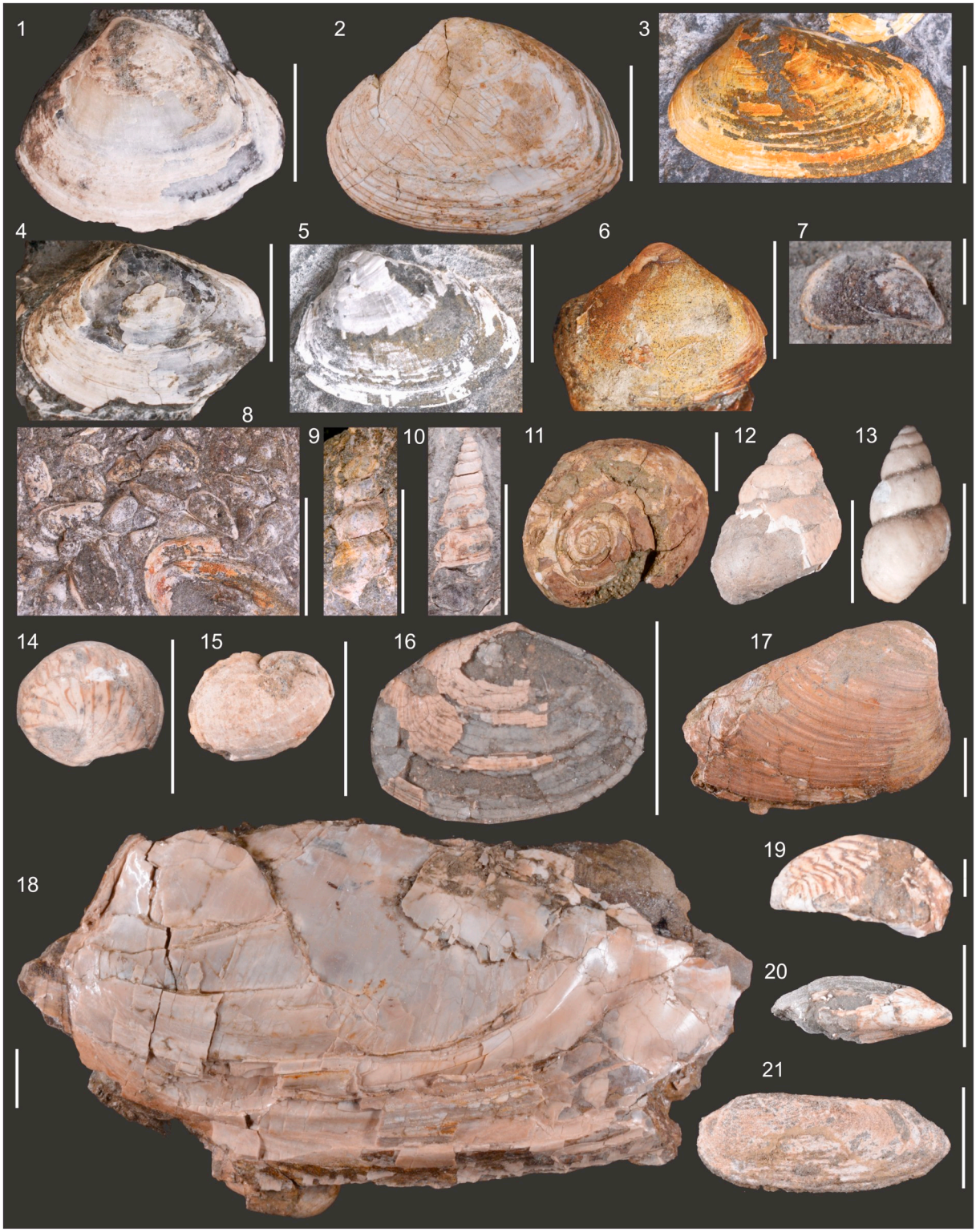

Fig. 5. Sarmatian s.l. (1 – 11) and Maeotian (12 – 21) molluscs from the Slănicul de Buzău section: 1–8 and 16–21 bivalves, 9–15 gastropods. Scale bars 10 mm, except for 7, 13 and 19–2 mm. 1–5. *Chersonimactra caspia* (samples 84–1 and 4, 91–2, and 92–3 and 5); 6. *Chersonimactra bulgarica* (sample 82); 7–8. *Coelogonia*? sp. (aff. *navicula*) (sample 86); 9–10. *Potamides*? sp. (cf. *disjunctus*) (sample 86); 11. *Helix mrazeci* (sample 91); 12. *Viviparus moldavicus* (sample 110b); 13. *Hydrobia vitrella* (sample 104); 14. *Theodoxus stefanescui* (sample 110b); 15. *Velutinopsis* sp. (sample 110b); 16. *Mactra superstes* (sample 102); 17. *Sinzowinaia subhoernesi* (sample 116a); 18. *Hyriopsis* cf. *krejcii* (sample 111); 19. *Andrussoviconcha modiolopsis* (sample 102); 20. *Dreissena polymorpha* (sample 110b); 21. *Dreissenomya rumana* (sample 109).

4.1.2. Stratigraphic interval 2 – Khersonian–Maeotian transition

Stratigraphic interval 2 (150.7–188.7 m) is dominated by claystones and siltstones of FA1 in combination with infrequent sandstones of FA3 and FA4 (Fig. 4, Table 1). It commences with yellow fissile siltstones that overlie the last red claystone of SI1 (Fig. 3B) and gradually develop into grey thickly-bedded low-angle cross-stratified sandstones

Table 2
Taxonomic composition, stratigraphic distribution and number of specimens per study sample of the mollusc fauna along the uppermost Khersonian–Maeotian interval of the Slănicul de Buzău section, and estimated palaeosalinity in the proximal depositional setting.

Stratigraphic level	2.5	56	62	62	69	81	151	195	229	231	259	264	278	604	659	713	726	934	934.5	963	964	968	997	1016	1034	1042	1053	1139	1186	1207	1244	1260
Taxon/Sample	82	91	92	84	85	86	90	87	89	88	99	100	101	102	103	104	105	116a	116b	110b	110a	110c	115	111	112	113	114	106	107	108	109	58
BRACKISH TO MARINE																																
Mactra superstes	-	-	-	-	-	-	-	-	-	-	-	-	-	10	-	-	-	-	-	-	-	-	-	-	-	-	-	-	-	-	-	-
Potamides? sp.	-	-	15	-	-	15	-	-	-	-	-	-	-	-	-	-	-	-	-	-	-	-	-	-	-	-	-	-	-	-	-	-
BRACKISH																																
Chersonimactra bulgarica	8	-	-	-	-	-	-	-	-	-	-	-	-	-	-	-	-	-	-	-	-	-	-	-	-	-	-	-	-	-	-	-
Chersonimactra caspia	-	35	35	43	10	25	-	-	-	-	-	-	-	-	-	-	-	-	-	-	-	-	-	-	-	-	-	-	-	-	-	-
Coelogonia? sp.	-	-	-	-	-	15	-	-	-	-	-	-	-	-	-	-	-	-	-	-	-	-	-	-	-	-	-	-	-	-	-	-
Andrusoviconcha modiolopsis	-	-	-	-	-	-	100	-	-	-	-	-	4	4	1	20	-	-	-	-	-	-	-	-	-	-	-	-	20	-	-	-
Leptanodonta rumana	-	-	-	-	-	-	-	-	-	-	-	-	-	-	-	-	-	-	-	-	-	-	-	-	-	-	-	-	-	-	29	6
BRACKISH TO FRESHWATER																																
Hydrobia vitrella	-	-	-	-	-	-	-	-	-	-	-	-	5	7	69	100	50	-	-	-	240	-	-	-	-	1	-	-	100	-	-	1
Pontohydrobia kelterborni	-	-	-	-	-	-	-	-	-	-	-	-	5	-	-	-	-	-	-	-	4	-	-	-	-	-	-	-	-	-	-	-
FRESHWATER																																
Anodonta sp.	-	-	-	-	-	-	-	-	-	-	-	-	-	-	1	-	-	-	-	-	-	-	-	-	-	-	-	-	-	-	-	-
Unio moldavicus	-	-	-	-	-	-	-	-	-	-	-	-	-	-	-	-	-	-	-	-	-	1	-	-	-	-	-	-	-	-	-	-
Teisseyrinaia subatava	-	-	-	-	-	-	-	-	-	-	-	-	-	-	-	-	-	-	-	-	-	4	-	-	-	-	-	-	-	-	-	-
Sinzowinaia subhoernesi	-	-	-	-	-	-	-	9	9	-	34	-	-	5	11	1	-	58	-	15	1	27	3	-	2	-	6	10	-	-	-	-
Hyriopsis cf. *krejcii*	-	-	-	-	-	-	-	-	-	-	-	-	-	-	-	-	-	-	1	-	-	-	-	2	-	-	-	-	-	1	-	-
Dreissena polymorpha	-	-	-	-	-	-	-	-	-	-	-	9	-	1	-	-	4	-	-	3	1	-	-	-	-	-	-	-	-	-	-	-
Theodoxus stefanescui	-	-	-	-	-	-	-	-	-	-	-	-	-	-	-	1	2	-	-	1	8	-	-	-	-	22	-	-	-			
Viviparus moldavicus	-	-	-	-	-	-	-	4	32	12	7	5	-	-	1	-	-	-	-	36	-	15	15	-	32	-	8	28	-	-	-	-
Lithoglyphus sp.	-	-	-	-	-	-	-	-	-	-	-	-	-	-	-	-	-	-	-	-	1	-	-	-	-	-	-	-	-	-	-	-
Velutinopsis sp.	-	-	-	-	-	-	-	-	-	-	-	-	-	-	-	-	-	-	-	3	4	-	-	-	-	-	-	-	-	-	-	-
TERRESTRIAL																																
Helix mrazeci	-	1	-	-	-	-	-	-	-	-	-	-	-	-	-	-	-	-	-	-	-	-	-	-	-	-	-	-	-	-	-	-
AGE	Khersonian						Maeotian																									
SALINITY	Brackish						Br.	Freshwater					Brackish				Freshwater											Br.	Fr.	Brackish		
STRATIGRAPHIC INTERVAL	1						2	3									4											5				

attributed to FA4. Further up, the sandstone is sharply covered by thinly-parallel-laminated siltstones of FA1. Slightly higher, at 156 m, a second remarkable sandstone package with gradational base and abundant ooids is exposed, which we attribute to FA3 (Fig. 4; Table 1). The latter is also sharply covered by siltstones of FA1 that continue until the end of SI2.

The only shell bed of SI2 occurs at 151.5 m and is composed of a monospecific assemblage of *Andrusoviconcha modiolopsis* (Table 2). The micropalaeontological assemblage of SI2 is dominated by the calcareous benthic foraminifera species *Ammonia beccarii*, associated with rare agglutinated foraminifera like *Miliammina subvelatina*, *Ammotium* sp. (Figs. 6, 7). Beside foraminifera, we identified the brackish-water ostracods: *Euxinocythere* (*Maetocythere*) *praebosqueti*, *Euxinocythere* (*Maetocythere*) *maeotica, Loxoconcha rimopora*, *Loxoconcha muelleri*, *Hemicytheria maeotica* and *Xestoleberis maeotica* (Figs. 6, 7). We also noticed an abundance of the euryhaline species *Cyprideis torosa*, as well as a few bryozoan fragments of *Tamanicella lapidosa* (Fig. 7).

4.1.3. Stratigraphic interval 3 – lower Maeotian

Stratigraphic interval 3 is characterized by alternations of sandstones and organic-rich claystones and can be subdivided into two subintervals: A lower part (188–329 m) with a predominant occurrence of FA2, FA3, FA4 and FA5 and an upper part (329–734.1 m) consisting mostly of FA1 and FA2 (Fig. 4, Table 1). While the lower part is exposed fairly continuously, the upper part contains a significant gap in exposure (370–600 m).

Stratigraphic interval 3 starts with some wave-ripple cross-laminated sandstones and thinly-laminated siltstones attributed to FA3 and FA2 respectively. These gradually pass into massive low-angle cross-laminated sandstones of FA4, followed by dark-grey organic-rich claystones with plant detritus attributed to FA5 (Table 1, Fig. 4). FA2 and FA3 dominate between 188 and 201 m, followed by an interval with predominant FA4 and FA5 (201–238 m). After a short (18 m) gap in the section, FA1, FA2 and FA3 return in the 256–273 m interval, while FA4 and FA5 govern the subsequent 273–329 m interval. The contact between FA4 and FA5 is usually sharp and the upper sandstone surface of FA4 is covered with ooids and broken shell fragments. At 220 m, FA5 is succeeded by a remarkable 1 m-thick coal layer attributed to FA9.

The upper part of SI3 (329–734.1 m) is mainly composed of claystones with rare bioturbated, convolute and wave-ripple cross-laminated sandstone packages (FA1, FA2 and FA3, Table 1). Several isolated sandstone bodies, attributed to FA2, have a sharp base and a well-developed set of sedimentary structures in upward order: parallel-lamination, convolute and soft-sediment deformation structures, climbing-ripple cross-lamination and eventually current-ripples developed on the sandstone top surface (625 m, 636 m, Fig. 4).

The mollusc fauna in SI3 was mainly found in the sandstone packages of FA3 and FA4. In the interval 195.5–264.2 m, a typical freshwater fauna with *Viviparus moldavicus*, *Sinzowinaia subhoernesi* and *Dreissena polymorpha* occurs (Fig. 5, Table 2). The overlying interval (278.3–726.9 m) contains *Mactra superstes*, brackish water hydrobiids – *Pontohydrobia kelterborni* and *Hydrobia vitrella*, as well as a few dreissenids, unionids, and viviparids (Fig. 5, Table 2).

The microfauna of SI3 comprises a low-brackish ostracod assemblage with some freshwater species (Fig. 6). The most common brackish water ostracod species are *Euxinocythere (Maetocythere) maeotica*, *Amnicythere mironovi*, *Amnicythere* sp., *Hemicytheria maeotica*, *Hemicytheria magna*, *Loxoconcha muelleri*, *Loxoconcha kochi*, *Loxoconcha rimopora*, *Limnocythere* sp., *Xestoleberis maeotica*, *Eucypris corrugate*, and euryhaline genus *Cyprideis torosa* (Fig. 8). Freshwater ostracods are represented by candoniid species like *Candona ricca*, *Candona bulgarica*, and *Candoniella* sp. (juveniles of *Candona* sp.) (Fig. 9).

4.1.4. Stratigraphic interval 4 – upper Maeotian

Stratigraphic interval 4 (915.7–1061.4 m) is separated from SI3 by a 182 m-thick gap in exposure (Fig. 4). SI4 begins with claystones of FA1 and FA2 that upwards gradually develop into hummocky cross-stratified sandstone (FA2), wave-ripple and low-angle cross-laminated sandstones (FA3–FA4) and bioturbated massive to fissile mudstones (FA5) (915.7–934.8,m, Fig. 4, Table 1). There subsequently is a distinctive, thick (< 8 m) sandstone bed with a sharp undulating base (FA8A, 934.8–942.8 m, Fig. 4, Table 1). Above this bed, there are repetitive successions that start either with grey thinly-parallel-laminated claystones (FA1) or with brown fissile mudstones (FA6), followed by thickening-upwards current-ripple and trough cross-laminated sandstones (FA7). In the upper part of SI4, this succession is repeatedly capped by a massive planar cross-bedded sandstone of FA8, the final one of which is thick (~6 m) and erosively based (Fig. 3F, G, Table 1). In the 1041–1043 m interval, there is furthermore a notable mudstone with a mottled aggregate structure (FA9, Fig. 4, Table 1), interbedded with thin sandstones.

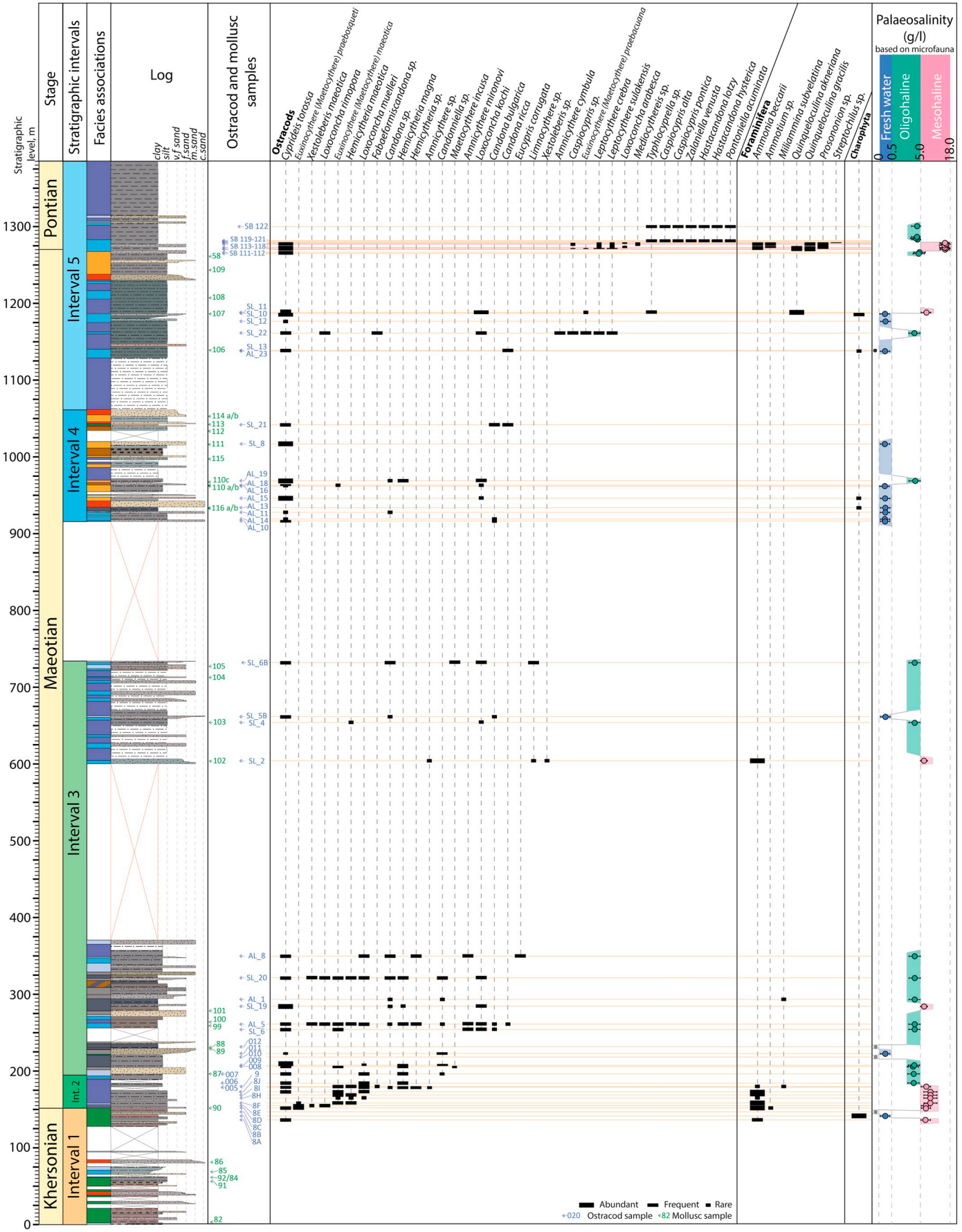

Fig. 6. Distribution of microfauna and estimated palaeosalinity in the distal setting of the Slănicul de Buzău section. The colour meaning in the facies association column is shown in the legend of Fig. 4.

Fig. 7. Microfossil assemblage from Stratigraphic interval 1 (uppermost Khersonian) and Stratigraphic interval 2 (Khersonian–Maeotian transition): 1–6. *Ammonia beccarii* (Linné); 7, 8. *Miliammina subvelatina* Venglinskij; 9, 10. *Ammotium sp.*; 11–13. *Hemicytheria maeotica* Olteanu; 14–16. *Cyprideis torosa* (Jones), smooth specimens; 17–19. *Loxoconcha rimopora* Suzin; 20,21. *Loxoconcha mulleri* (Méhes); 22–24. *Euxinocythere (Maetocythere) praebosqueti* Suzin; 25–27. *Euxinocythere (Maetocythere) maeotica* (Livental); 28–30. *Xestoleberis maeotica* Suzin; 31, 32. *Tamanicella lapidosa* (Pallas); 33–36. *Nitellopsis (Tectochara) meriani* (Braun ex Unger) - charophyte algae gyrogonites.

The mollusc fauna observed within SI4 is mostly situated between the thin current-ripple cross-laminated sandstone beds of FA7, and represented by a rich freshwater association with *Dreissena polymorpha*, *Sinzowinaia subhoernesi*, *Unio moldavicus*, *Teisseyrinaia subatava*, *Hyriopsis* cf. *krejcii*, *Theodoxus stefanescui*, *Viviparus moldavicus*, *Lithoglyphus* sp., *Velutinopsis* sp. (Table 2, Fig. 5). At 964.3 m, a remarkably high number of *Hydrobia vitrella* was found in the grey siltstones.

The micropalaeontological association of SI4 is dominated by freshwater ostracods, but also contains a few brackish water species.

Fig. 8. Brackish ostracods and foraminifera from Stratigraphic interval 3 (lower Maeotian) and Stratigraphic interval 4 (upper Maeotian): 1–3. *Cyprideis torosa* (Jones), smooth specimens; 4–6. *Eucypris corrugata* Stancheva; 7–9. *Hemicytheria magna* Olteanu; 10–12. *Hemicytheria maeotica* Olteanu; 13–15. *Xestoleberis meotica* Suzin; 16–18. *Euxinocythere (Maetocythere) maeotica* (Livental); 19–21. *Amnicythere. mironovi* (Schneider); 22–24. *Loxoconcha kochi* Méhes; 25–27. *Loxoconcha rimopora* Suzin; 28–30. *Loxoconcha mulleri* (Méhes); 31–33. *Ammotium* sp.; 34–36. *Miliammina subvelatina* Venglinskij.

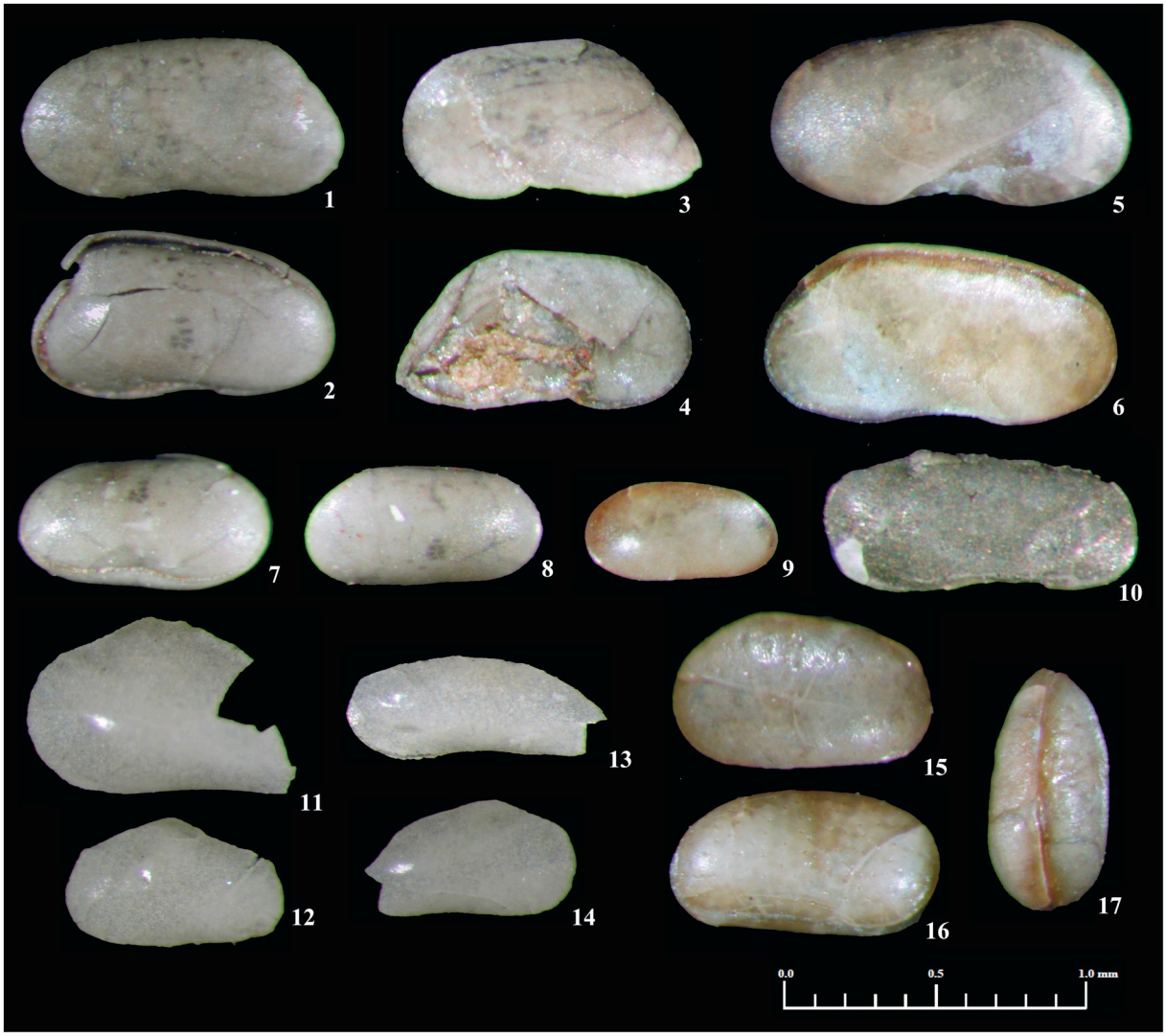

Fig. 9. Freshwater ostracods from Stratigraphic interval 3 (lower Maeotian) and Stratigraphic interval 4 (upper Maeotian): 1, 2. *Candona ricca* Stancheva; 3, 4. *Candona bulgarica* Stancheva; 5, 6. *Candona* sp.; 7–9. *Candona* sp. juveniles, frequent named as *Candoniella* sp.; 10. *Fabaeformiscandona* sp. (internal pyritized cast); 11, 12. *Eucypris* sp. (fragmented valves); 13, 14. *Typhlocyprella* sp. (fragmented valves); 15–17. *Cyprideis torosa* (Jones).

Characteristic for this interval is the abundance of the euryhaline species *Cyprideis torosa*, frequently with shells filled with secondary calcite (Fig. 8). The candoniid ostracods are represented by *Candona* sp. (mostly in juvenile stages recorded as *Candoniella* sp.), rare *Candona ricca*, *Candona bulgarica*, and *Eucythere corrugata* (Fig. 9). The only interval with brackish ostracods (969.9 m) contains a few specimens of *Hemicytheria magna, Loxoconcha muelleri*, *Loxoconcha kochi*, *Limnocythere* sp. (Fig. 6).

4.1.5. Stratigraphic interval 5 – Maeotian–Pontian transition

Stratigraphic interval 5 (1061.4–1380 m, Fig. 4) mainly consists of bluish-grey fissile, thinly-parallel-laminated claystones (FA1) that abruptly cover the final distinct FA8 sandstone of SI4 (Fig. 4, Table 1). The claystones are often interbedded with 0.2–1 m-thick sandstone packages with various sedimentary structures. Some of these sandstones have a gradual base and display planar cross- and low-angle cross-lamination and are thus attributed to FA2 (Fig. 4, Table 1). Other sandstones are sharp-based and display low-angle or parallel-lamination at the base, climbing ripples and convoluted bedding in their middle part and current- or wave-ripples in their upper part (1175–1187 m, Fig. 4). These sandstones were previously noted in SI3 (625 m, 636 m) and attributed to FA2.

At 1230 m, a massive sharp-based thickly-bedded planar cross-laminated FA8B-type sandstone with plant detritus and mud drapes disrupts the claystone record (Fig. 4). Above the FA8B sandstone, there are frequent sharp-based trough-cross laminated FA7 sandstones (1237.7–1267 m). The siltstones directly underlying these beds demonstrate soft-sediment deformation structures. In interval 1267–1282 m, the sandstones show either parallel-lamination or rarely wave-ripple cross-lamination and hence were assigned to FA2 (Table 1). Further up, the section shows mainly parallel-laminated claystone (FA1) with some rare sandstone beds (FA2, FA3, Fig. 3).

The mollusc fauna of Interval 5 mainly occurs in sandstone beds. Between 1139 m and 1186.8 m, there is a freshwater assemblage with *Sinzowinaia subhoernesi* and *Viviparus moldavicus* (Fig. 5). Starting from 1186.8 m, the mollusc fauna contains brackish water assemblages with *Andrusoviconcha modiolopsis*, *Hydrobia vitrella and Leptanodonta rumana* (Fig. 5, Table 2). From 1265 m, remarkable thin (5–15 cm) shell beds with brackish water *Coelogonia novorossica* occur (Fig. 10). These beds continue in the record until 1286 m, where the first *Eupatorina littoralis* occurs.

The microfauna of SI5, like the mollusc fauna, demonstrates a change from freshwater to brackish water assemblages. In the interval 1139–1166 m, a freshwater microfauna assemblage with *Candona ricca*,

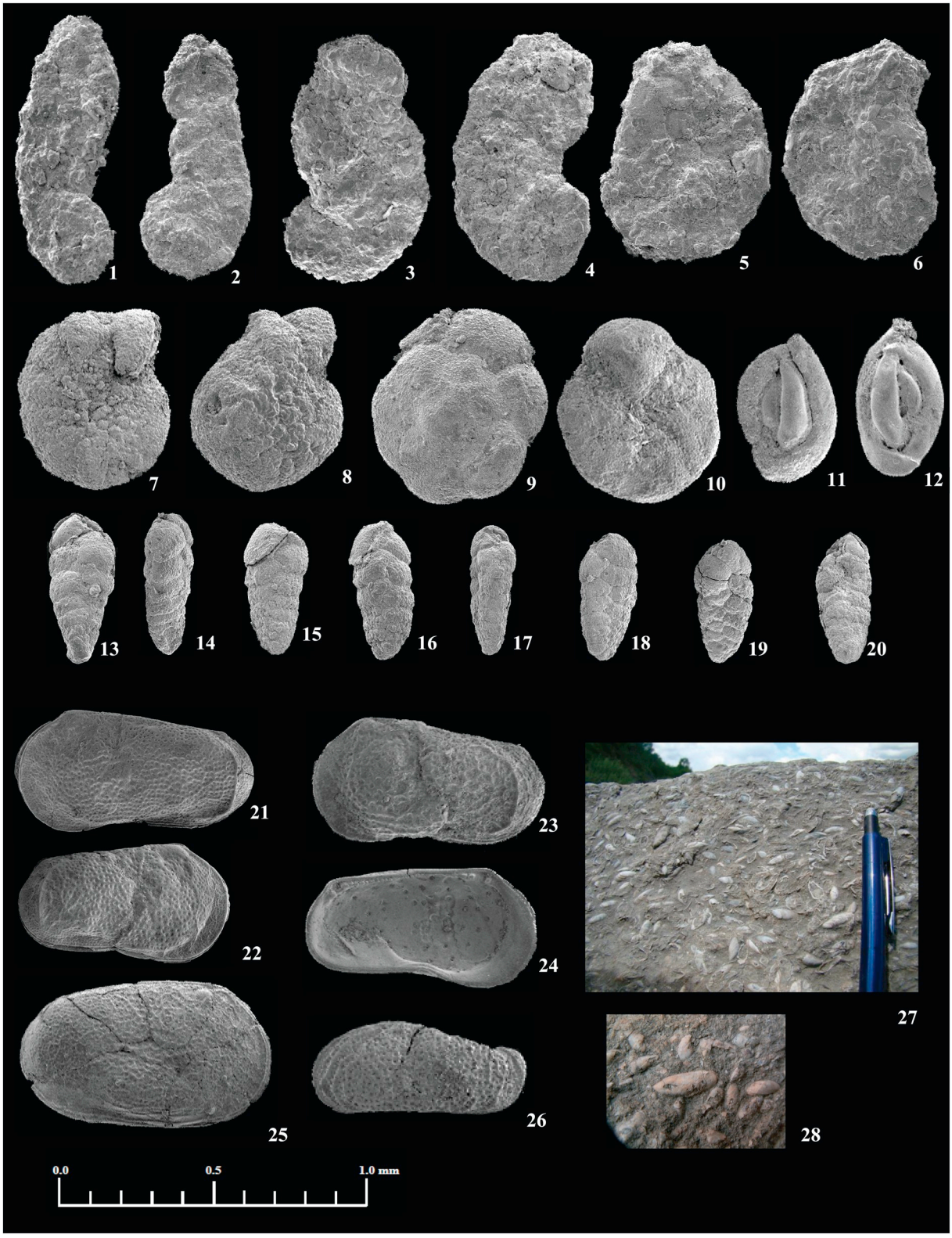

Fig. 10. Foraminifera, ostracods and bivalves from Stratigraphic interval 5 (upper Maeotian – lower Pontian) and Maeotian–Pontian boundary (Flooding interval) 1–6. *Ammotium sp.,* different morphotypes; 7, 8. *Porosononion sp.* 9,10.*Ammonia* ex.gr. *beccarii* (Linné); 11,12. *Quinqueloculina* aff. *Gracilis* Karer; 13–20. *Streptochilus* sp. (bad preserved specimens); 21, 22. *Leptocythere* aff. *Sulakensis* Suzin; 23, 24. *Leptocythere* aff. *Crebra* Suzin; 25. Loxoconcha arabesca Olteanu; 26. *Mediocytheries* sp.; 27, 28. Shell accumulation with *Coelogonia novorossica* (Andrusov).

Cyprideis torosa and gyrogonites of *Nitellopsis* sp. is present (Fig. 6). At 1166 m, a brackish water assemblage with *Cyprideis torosa*, *Leptocythere crebra*, *Leptocythere sulakensis*, *Euxinocythere praebacuana*, *Amnicythere cymbula, Loxoconcha kochi*, *Loxoconcha muelleri* occurs (Figs. 6, 10). At 1186.8 m, we discovered an assemblage dominated by the foraminifera *Quinqueloculina* sp. and the fragile (mainly fragmented) ostracod

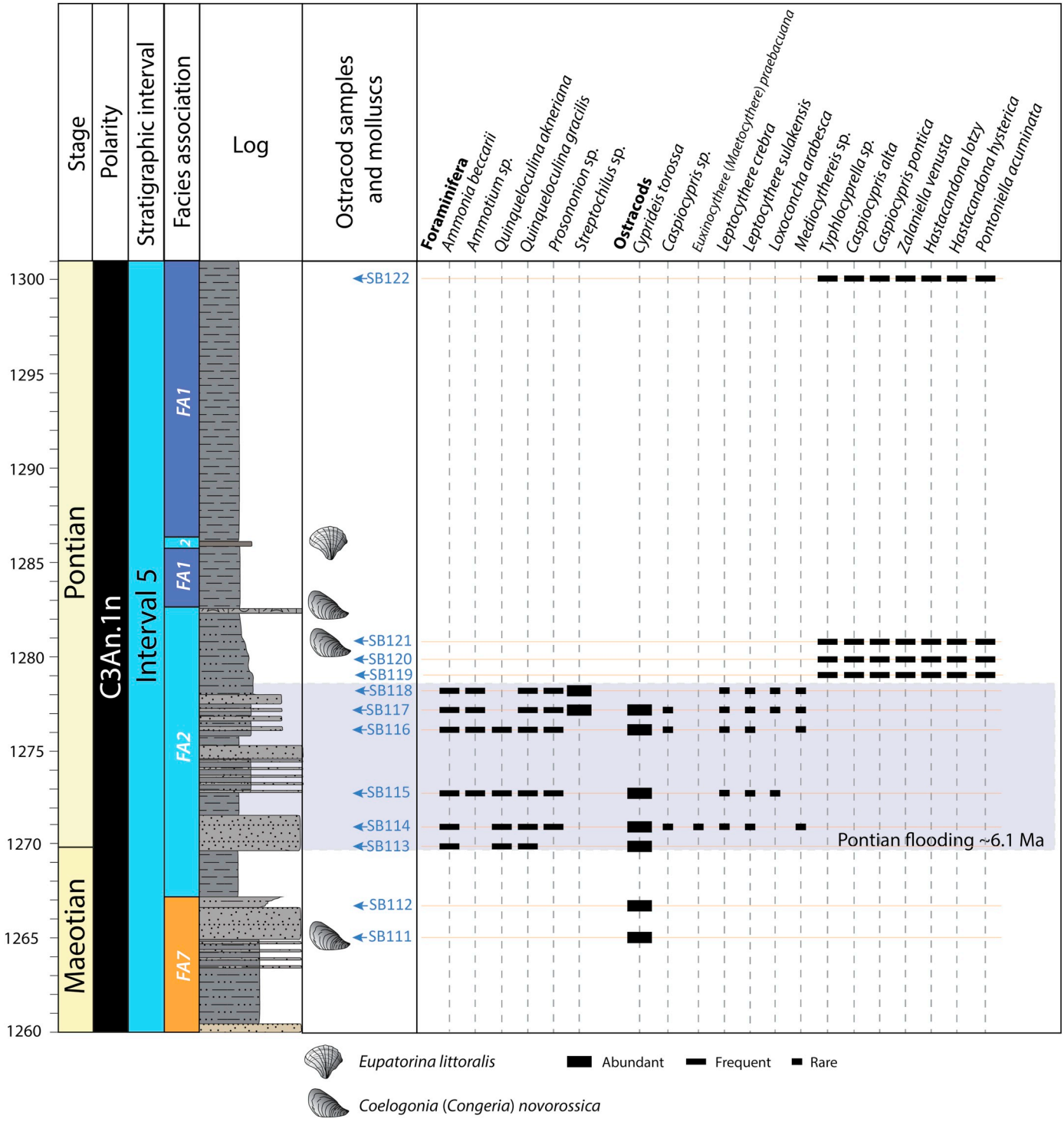

Fig. 11. Magneto-biostratigraphic characteristic of the Maeotian–Pontian boundary in the Slănicul de Buzău section. The colour meaning in the facies association column is shown in the legend of Fig. 4.

Typhlocyprella sp. (Fig. 6).

Starting from 1265 m, high-resolution micropalaeontological sampling was performed (Fig. 11). In the interval 1265–1270 m (SB111–SB112), a low-brackish water monospecific assemblage with *Cyprideis torosa* was discovered. Between 1270 m and 1278 m (SB113–SB118), a very different meso- to polyhaline microfauna is present, characterized by abundant foraminifera like *Ammonia beccarii*, *Ammotium* sp., *Quinqueloculina akneriana*, *Q. gracilis*, *Prosononion* sp. and *Streptochilus* sp. and the ostracods *Caspiocypris* sp., *Euxinocythere* (*Maetocythere*) *praebacuana*, *Leptocythere crebra*, *L. sulakensis*, *Loxoconcha arabesca* and *Mediocythereis* sp. (Figs. 10, 11). The following interval 1279–1300 m (SB119–SB122) contains no foraminifera, but a low-brackish water ostracod assemblage with *Caspiocypris alta*, *Caspiocypris pontica*, *Zalaniella venusta*, *Hastacandona lotzy*, *H. hysterica*, *Pontoniella acuminata* and *Typhlocyprella* sp. (Figs. 8, 10, 11).

4.2. Magnetostratigraphy

Demagnetization of 157 samples with alternating field and/or thermal methods revealed two magnetic components. The first

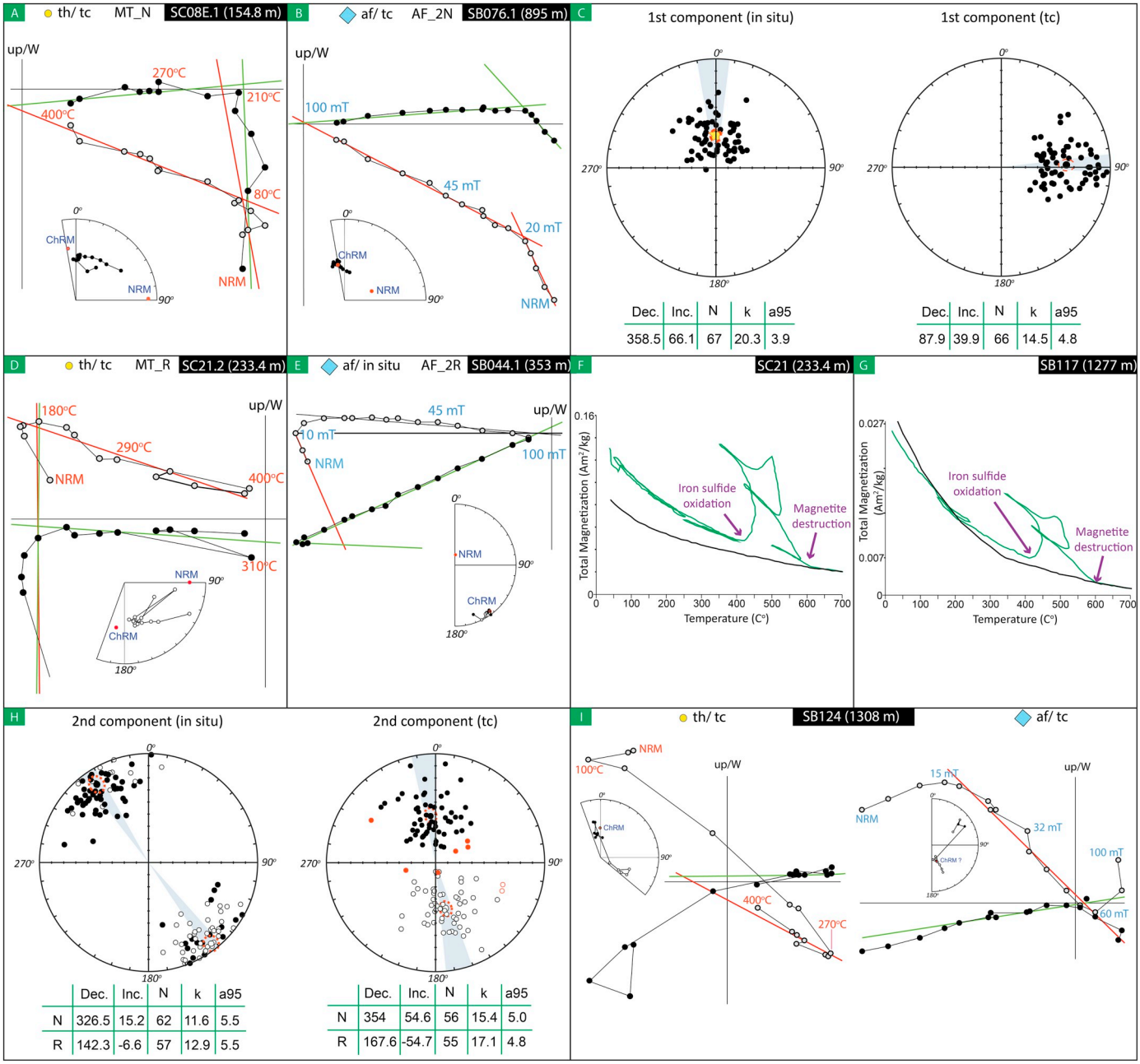

Fig. 12. Zijderveld diagrams, equal-area plots and thermomagnetic curves for samples from the Slănicul de Buzău section. Zijderveld diagrams with representative 1st magnetic component for: A. thermally demagnetized samples (0–210 °C); B. demagnetized in alternating field samples (0–20 mT); with representative 2nd magnetic component for: D. thermally demagnetized samples (180–400 °C); E. demagnetized in alternating field (20–100 mT). Equal are plots of the: C. 1st magnetic component in geographic (in situ) and in tectonic (tc) coordinates; H. all normal and reversed ChRM direction (2nd magnetic component) in geographic (in situ) and tectonic (tc) coordinates. The yellow star represents the current day GAD direction of the studied area. Thermomagnetic runs showing different magnetic carriers: F and G. Pyrite and magnetite; I. Zijderveld diagrams showing the antipodal directions in the sample with two generations of greigite: diagenetic (100–270 °C or 20–60 mT) and characteristic (270–400 °C or 60–100 mT). Abbreviations and parameters: th – thermally demagnetized; af – demagnetized in alternating field; tc – tectonically corrected coordinates; in situ – geographic coordinates; NRM – natural remanent magnetization; ChRM - characteristic remanent magnetization; Dec. – declination; Inc. – inclination; N – number of samples; k – precision parameter of Fischer, a95–95% cone of confidence; MT_N and MT_R – medium temperature component with normal and reversed direction correspondingly; AF_2N and AF_2R – alternating field demagnetized component with normal and reversed direction correspondingly. (For interpretation of the references to colour in this figure legend, the reader is referred to the web version of this article.)

magnetic component is demagnetized between 180 °C and 210 °C for thermal measurements (TH) and between 20 mT and 25 mT for measurements in alternating field (AF) (Fig. 12A, B). The combined mean direction of the first component for both AF and TH measurements, has parameters of D = 358.5°, I = 66.1°, k = 20.3, α95 = 3.9 for N = 67 samples in geographic coordinates (Fig. 12C) For the Slănicul de Buzău area, the expected direction of the geocentric axial dipole (GAD) field is I = 63°, which is close to the measured inclination of the first component. We therefore interpret the first component to represent the present-day magnetic field overprint.

The second magnetic component most commonly demagnetizes between 400 °C and 440 °C (TH) or between 60 mT and 80 mT (AF) (Fig. 12D, E). The thermomagnetic runs show a decrease of magnetization up to 420–440 °C and subsequently form a peak that drops off at

580 °C (Fig. 12F, G). Such behaviour and the curve shape are typical for the oxidation of pyrite followed by magnetite demagnetisation. The combined mean direction for all normal samples demagnetized thermally and in alternating field has parameters of D = 354°, *I* = 54.6°, k = 15.4, a95 = 5.0 for *N* = 56 in tectonic coordinates, while for all reversed directions combined the parameters are D = 167.6°, *I* = −54.7°, k = 17.1, a95 = 4.8 for *N* = 55, equally in tectonic coordinates (Fig. 12H). Both, the classical (McFadden and McElhinny, 1990) and the bootstrap (Tauxe, 2010) reversal tests are positive for the second magnetic component. Therefore, the second magnetic component is interpreted as characteristic remanent magnetisation (ChRM) and as a primary component being characteristic for the depositional age of the sediment.

The two antipodal NRM directions have been detected in some rare samples from SI5 (Fig. 12I). The first of these two directions demagnetizes at 270–290 °C, while the second one demagnetizes at 360–400 °C. These demagnetization temperature ranges are characteristic for greigite. Antipodal directions are known from the Dacian Basin and linked to two different greigite generations: the low-temperature authigenic and the high-temperature magnetosomal (Vasiliev et al., 2008; Kelder et al., 2018). The low-temperature diagenetic greigite formed later than the magnetosomes and thus acquired a later magnetic field (Vasiliev et al., 2008). For the determination of a true magnetic signal we used the second, high-temperature greigite directions, whose polarity is in accordance with the other samples below and above, which only have a ChRM component.

The magnetostratigraphic record of the studied interval in Slănicul de Buzău consists of three normal zones and four major reversed zones, two of which are interrupted by some unexposed intervals (Fig. 13). The section starts with reversed zone R1a that is followed by a gap between 95.8 m and 127.6 m. After the gap, the upper part of SI1 begins with the reversed polarity zone R1b (127.6–138.3 m) and after that, the normal zone N1 covers the rest of SI1, SI2 and the lower part of SI3 (139.3–228.2 m). Within the normal zone, a short reversed level (345.5–348.5 m) has been detected that we interpret as an anomaly. Between normal zones N1 and N2, the magnetostratigraphic record is represented by the long R2 reversed zone that consists of R2a (228.2–386 m), R2b (516 m), R2c (596–728 m) separated by three major gaps (Fig. 13). Upwards from normal zone N2 (890?–952.5/974 m), which has an ill-defined lower limit, the section is fairly continuous. In the middle part of SI4, the reversed zone R3 (952.5/974–1085 m) occurs and is succeeded by a long normal zone N3 (1085–1362 m) that switches to reverse R4 at 1362 m (Fig. 13).

4.3. Palaeoenvironmental interpretation

The interpretation of depositional environments is based on sedimentary facies analysis (Table 1), supported by the associated microfauna and molluscs. Salinity trends are reconstructed based on palaeoecology of ostracod and mollusc assemblages. The frequent occurrence of chaotically distributed mollusc fauna in sandy layers suggests that they were transported downslope from a shallower setting. Analysis of these mollusc assemblages provides an estimation of salinity in the marginal, shallow water parts of the basin. The ostracod fauna present in relatively deep-water offshore mud deposits is considered as a representative indicator of salinity in the distal parts of the basin. For our estimation of salinity we use the Venice system with freshwater (0–0.5 g/l), oligohaline (0.5–5 g/l), mesohaline (5–18 g/l) and polyhaline (18–30 g/l) ranges (The Venice System for the Classification of Marine Waters According to Salinity, 1958).

4.3.1. Stratigraphic interval 1 – upper Khersonian

We interpret the lower and upper parts of SI1 with the sandstone-grey mudstone-red claystone packages as being deposited in coastal lagoons and floodplains (FA9) that were subject to small periodic transgressions (Table 1). The red palaeosols with scarce freshwater oogonides were formed on floodplains. The sandstone packages with wave ripples and planar cross-lamination represent coastal barriers and crevasse splays, respectively. The limestones with *Chersonimactra* shells (lower part of SI1) and the massive mudstones with abundant *Ammonia beccarii* foraminifera (upper part of SI1) reflect occasional brackish water transgressions of the coastal plain.

The middle part of SI1 was formed in littoral environments ranging from offshore to shoreface (FA1–FA3, Table 1). The parallel-laminated siltstones accumulated in a quiet offshore setting with a lack of bioturbation, probably due to weak oxygenation. The upper beds of these packages with wave-ripples and low-angle cross-lamination characterize deposition on a shoreface with a marked wave activity (FA3, Table 1). The highly erosive fining-upward sandstone body (81–84 m) with intraformational breccia at the base is interpreted as a channel with diminishing activity towards the top (FA8A, Table 1).

The mollusc fauna found within the lower and middle parts of SI1 is indicative for the Khersonian (sub)stage of the Eastern Paratethys (Paramonova, 1994). The occurrence of the euryhaline genus *Chersonimactra* together with *Coelogonia*? sp. and *Potamides*? sp., suggest an oligo- to mesohaline salinity for the coastal lagoons and nearshore (shoreface) part of the basin (Table 2). *Helix mrazeci* is terrestrial and its co-occurrence with *Sarmatimactra bulgarica* at 56 m points at the proximity of shallow marine and terrestrial depositional environments.

The upper part of SI1 lacks mollusc fauna, but displays an alternation of intervals with brackish water foraminifera, freshwater oogonides and small barren intervals. The association of *Ammonia beccarii* and the euryhaline *Cyprideis torosa*, which occur in lagoon mudstones, indicates a lower mesohaline salinity (5–7 g/l.) We thus interpret the upper Khersonian (SI1) to have been deposited in coastal lagoon and floodplain environments, shortly interrupted by littoral conditions.

4.3.2. Stratigraphic interval 2 – Khersonian – Maeotian transition

At the onset of SI2, there is a major transition from coastal plain (FA9) to offshore (FA1) depositional settings. The gradual transition from yellow siltstone (FA9) into low-angle cross-stratified sandstone (FA4) at the base of SI2 (150.8–153 m) indicates a landward-retreat of the coastal barrier, thus covering previously deposited lagoon sediments due to a rise of relative water level (Table 1) (McCubbin, 1982). The overlaying thinly-parallel-laminated siltstones, characteristic for most of SI2, were deposited in a low-energy environment beneath storm-wave base and with a low biological activity, which we interpret as offshore (FA1, Table 1). The sharp contact between the barrier sandstone and overlying offshore siltstones indicates a drowning of the back barrier-lagoon system (McCubbin, 1982). The second sandstone package with ooids (FA3, 155.7–157.7 m, Fig. 1) suggests a temporary return to shoreface environments with a constant agitation by wave processes and high saturation of water with calcium carbonate (Flügel, 2010).

The presence of *Andrusoviconcha modiolopsis* in the shoreface deposits at 151.5 m suggests a mesohaline salinity for the marginal parts of the basin. The almost exclusive presence of euryhaline foraminifera *Ammonia* in the offshore deposits, with no other calcareous foraminifera implies a mesohaline salinity below 10 g/l. The agglutinated foraminifera of the genera *Miliammina* and *Ammotium* can also tolerate very low salinity.

4.3.3. Stratigraphic interval 3 – lower Maeotian

The wave-ripple cross-laminated sandstone (188 m) at the base of SI3 indicates a shoreface setting (FA3) that passes upwards into a barrier sandstone (201–204.8 m, FA4, Table 1). The occurrence of ooids and broken shells on the barrier top surfaces indicate a weak wave activity on the internal side of the barriers and water highly saturated in calcium carbonate (Flügel, 2010). The following dark-grey claystones with plant detritus represent lagoons that were trapped by barrier islands and preserved the organic matter. The distinctive shallowing trend (FA3-FA4-FA5) reaches its maximum at 220 m where a 1 m-thick

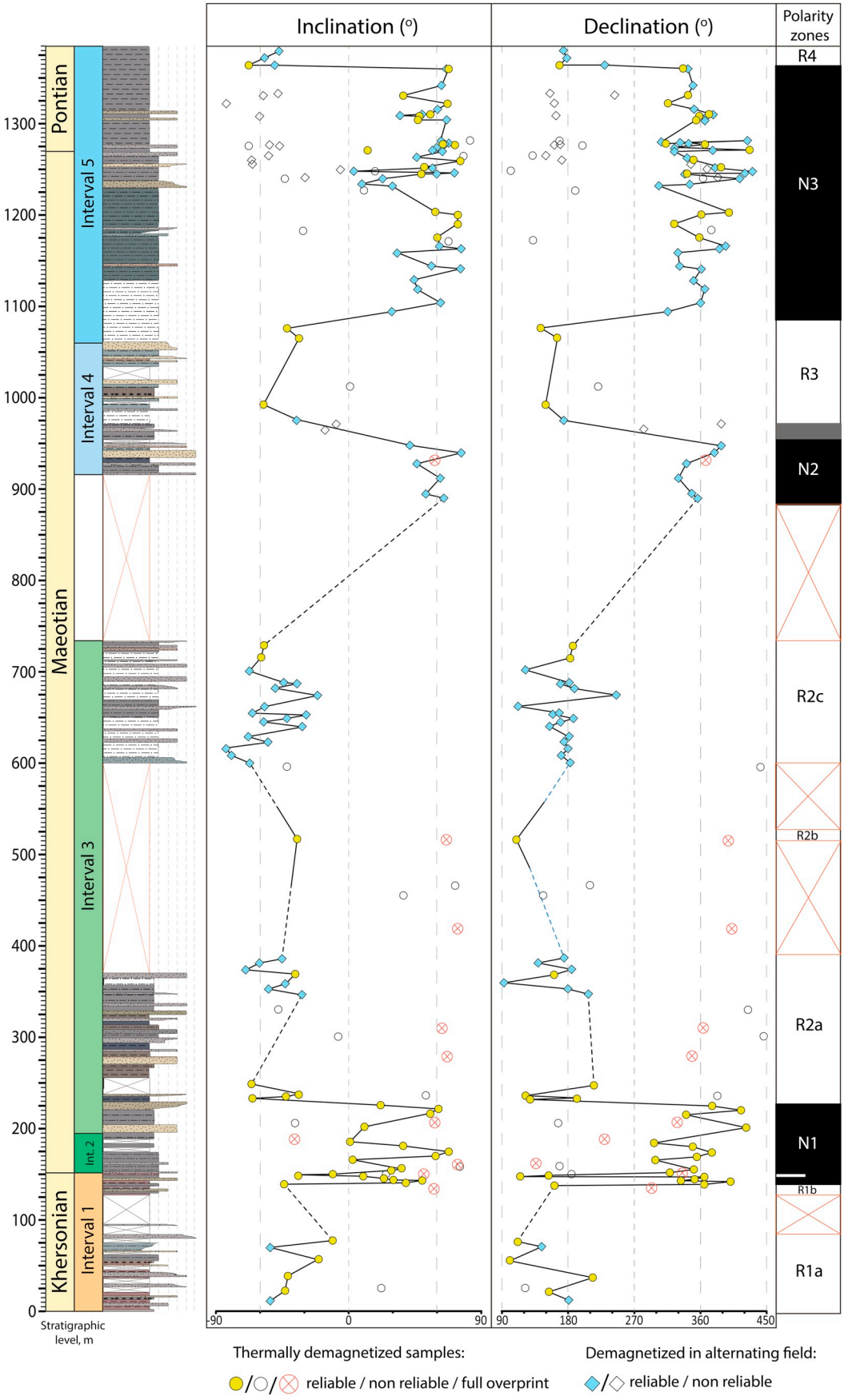

Fig. 13. Magnetic polarity pattern identified in the Slănicul de Buzău section.

coal layer attributed to FA9 indicates a swampy, subaerially exposed environment. Subsequently lagoon and barrier deposits alternate up to 238 m. Following a short (18 m) gap in the section, there is a return to offshore-transition and offshore deposits (FA2 and FA1) in the 251–271 m interval, after which the barrier-lagoon system returns, persisting up to 329 m. Within this FA4-FA5 package there is a distinctive thick sandstone barrier (294–300 m, Fig. 3C) that covers lagoon deposits with a sharp basal surface dotted with *Diplocraterion* burrows (Fig. 3E).

The lower back-barrier lagoon (FA4–FA5) succession and the following short offshore-shoreface interval (195–271 m) contain a typical freshwater mollusc assemblage with *Viviparus moldavicus*, *Sinzowinaia subhoernesi* and *Dreissena polymorpha* (Fig. 5, Table 2) and a freshwater to low brackish water ostracod assemblage with *Cyprideis torosa*, *Candoniella* sp., *Candona neglecta* (Fig. 6). The mollusc fauna in the second FA4-FA5 succession (271–329 m) contains low brackish water molluscs *Andrusoviconcha modiolopsis*, *Hydrobia vitrella*, *Pontohydrobia kelterborni* (278 m, Table 2) and numerous brackish water ostracod species (Fig. 6). Thereby, the lower Maeotian back-barrier lagoon system developed in freshwater to oligohaline (up to 5‰) environments.

Following an interval with FA3 and FA2, interpreted as shoreface and offshore transition zone respectively (329–348 m), the whole upper part of SI3 (348–734 m) is dominated by FA1 facies interpreted as representative of the offshore (Fig. 4, Table 1). The thick single-bed sandstones with well-developed soft-sediment deformation structures and climbing-ripple cross-lamination (625 m, 636 m, Fig. 4) represent a rapid deposition from uni-directional sediment-laden flows that resulted from exceptional storm events (Ashley et al., 1982; Oliveira et al., 2011). The gradually-thickening bioturbated sandstone packages with low-angle cross-lamination and locally wave-ripple marks (e.g. 655.5–661 m, Fig. 4) are interpreted to have formed under the influence of storms and wave activity, suggesting an offshore transition (FA2) or shoreface (FA3) origin.

The mollusc fauna from this upper part of SI3 contains brackish water assemblages with minor freshwater elements: *Mactra superstes*, *Andrusoviconcha modiolopsis*, *Hydrobia vitrella*, *Sinzowinaia subhoernesi,* etc. (Table 2). The microfauna from the upper part of SI3 is represented by oligohaline species with, however, a taxonomic and quantitative decrease (Fig. 6).

4.3.4. Stratigraphic interval 4 – upper Maeotian

The base of SI4 (915.7–942.8 m, Fig. 4) consists of a shallowing-upwards succession from offshore (FA1) to shoreface (FA3) and back-barrier lagoon (FA4–FA5), followed by the arrival of a large distributary channel (FA8, Fig. 4). The thinly-parallel-laminated claystones (FA1) suggest accumulation in a quiet offshore setting below the storm wave base. The following thickly-bedded hummocky cross-stratified sandstone reveals storm wave activity within the offshore transition zone (FA2). The overlying wave-rippled sandstone points at active wave generated motions and thus suggests accumulation on the shoreface (FA3). The succeeding low-angle cross-bedded sandstones with structureless organic-rich mudstones are interpreted as a back-barrier lagoon system (FA4–FA5) with a distributary channel on top (FA8) (Table 1). Interpretation of the latter is supported by its erosive base and a well-developed intraformational mud clast breccia suggesting erosion (collapse) of the upstream mud-ground. It also contains a transition from planar cross-lamination through trough cross-lamination to current ripples, characteristic for the diminishing energy of deposition in a laterally migrating distributary channel.

The overlying 945–1061 m interval shows 7 repetitions of a typical shallowing-upwards succession (e.g. Fig. 3F). These successions start either with grey thinly-parallel-laminated claystones (FA1) or with brown fissile mudstones (FA6) interpreted to be deposited from suspension fallout in offshore and prodelta environments below the wave base (Table 1, Fig. 4). The overlying thickening-upwards current-ripple and trough cross-laminated sandstones (FA7) are interpreted as the prograding delta front. While the lower 4 successions terminate on the distal delta front, the 5th succession terminates on the proximal delta front and the final two successions terminate with mouth bar (FA8B) to channel (FA8A) facies. These 7 cyclic shallowing-upwards successions are interpreted as a progradational set of deltaic parasequences (e.g. Jorissen et al., 2018), culminating in mouth-bar (FA8B, erosively based channel (FA8A) and red, mottled palaeosol (FA9) deposits in the final two parasequences.

The mollusc fauna of SI4 consists of freshwater species like *Sinzowinaia subhoernesi*, *Unio moldavicus*, *Teisseyrinaia subatava*, *Hyriopsis* cf. *krejcii*, *Theodoxus stefanescui*, *Viviparus moldavicus* (Fig. 5, Table 2), which are considered typical for the upper Maeotian (Wenz, 1942; Roshka, 1973; Paramonova, 1994). In our section, this fauna is distributed in the delta front and delta top depositional settings, where the occurrence of freshwater forms is expected. The domination of *Candona* sp. in offshore deposits (Fig. 6) and a scarce occurrence of brackish water molluscs and ostracods (964.3 m, Fig. 6 and 969.9 m, Table 1) suggests strong freshening of the basin margins and a probably very low brackish (low oligohaline) salinity of the more distal parts of the basin.

4.3.5. Stratigraphic interval 5 – Maeotian–Pontian transition

Stratigraphic interval 5 is interpreted to have been mainly deposited in the offshore (Fig. 4, Table 1). The fissile planar parallel claystones and siltstones (FA1) were deposited in quiet environments, beyond storm and wave activity. The single sandstones (FA2), sporadically occurring among the claystones, are interpreted to have been deposited from uni-directional sediment-laden flows towards the offshore, generated during exceptional storms. The massive planar cross-laminated sandstone at 1230 m does not have an erosive base and is interpreted as a mouth bar deposit (FA8B). It is overlain by thin sandstone beds deposited on the delta front (FA7, Table 1). The following sandstones of interval 1267–1282 m accumulated in an offshore transition setting (FA2, Table 1). Subsequently, the sandstones disappear and offshore depositional settings prevail until the end of the studied section.

Both molluscs and microfauna indicate fresh water in the lower part of SI5. Starting from 1166 m, some brackish water pulses are indicated by *Quinqueloculina* sp. and fragile candonid ostracods (mainly fragmented) *Typhlocyprella*, which alternate with layers containing freshwater molluscs. At 1265 m, *Coelogonia novorossica* and *Cyprideis torosa* suggest an oligohaline salinity. The abundance of foraminifera between 1270 and 1278 m indicates an abrupt rise of salinity to meso- polyhaline values (Fig. 11), which is followed by an interval with oligohaline ostracods (1279–1300 m).

5. Discussion

5.1. Magneto-biostratigraphic correlation to the GPTS

The incompleteness of the record in the middle part excludes a straightforward correlation of the acquired polarity pattern to the GPTS (Fig. 14). However, the lower and upper parts where the stage boundaries are exposed can be used as important tie-points.

The Maeotian–Pontian boundary is characterized by the occurrence of new marine assemblages of ostracods, foraminifers, nannoplankton and molluscs that entered the Paratethys region from the Mediterranean and Lake Pannon (Stevanovic et al., 1989; Krijgsman et al., 2010; Popov et al., 2016; Stoica et al., 2016). This influx of marine fauna, called the “Pontian flooding”, was correlated magnetostratigraphically slightly below the C3An.1n–C3r polarity switch and dated in the Dacian Basin at 6.04 Ma (Krijgsman et al., 2010). Cyclostratigraphic calibration of this boundary in the Caspian and Black seas suggest a 6.1 Ma age (Chang et al., 2014; van Baak et al., 2016; Rostovtseva and Rybkina, 2017). We place the Maeotian–Pontian boundary in Slănicul de Buzău at 1270 m (Sample SB113), in the upper part of normal zone N3, where we note the sudden appearance of a

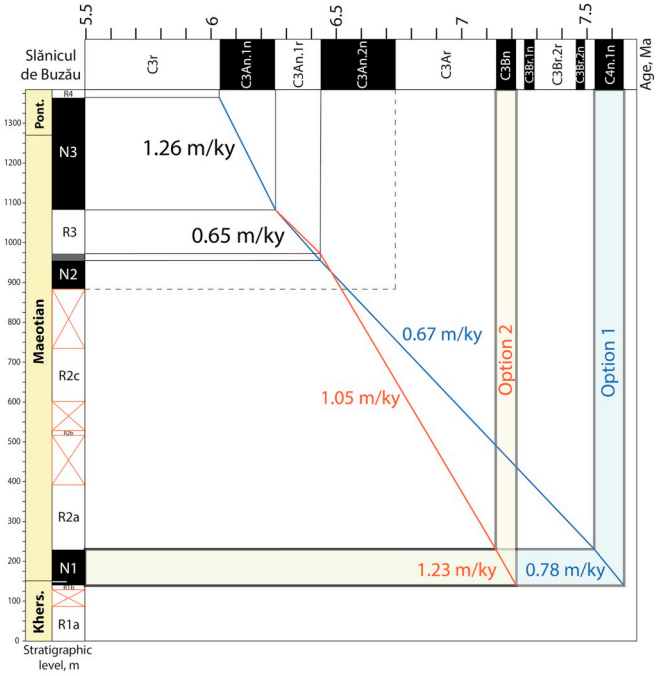

Fig. 14. Correlation of polarity patterns to the Geomagnetic Polarity Time Scale (GPTS) and estimated sedimentation rates with two possible options.

remarkable meso-, polyhaline microfauna followed by the appearance of typical Pontian molluscs at 1286 m (Fig. 11). Considering the position of the Maeotian – Pontian boundary in the regional GTS, we correlate the normal zones N2 and N3 from the Slănicul de Buzău section to the C3An.2n and C3An.1n subchrons, respectively. This correlation results in a 6.1 Ma ± 5 kyr age for the Maeotian-Pontian boundary in our section.

However, there is a small discrepancy with the age of 6.04 Ma that was earlier acquired from the Rîmnicu Sărat section in the Dacian basin (Vasiliev et al., 2004; Krijgsman et al., 2010; Stoica et al., 2013; Stoica et al., 2016). In the Rîmnicu Sărat section, the polarity switch was placed at the first reversed sample followed by a 100 m non-sampled, poorly exposed interval (Vasiliev et al., 2004). The high-resolution palaeomagnetic record of Slănicul de Buzău revealed a series of single reversed samples within the normal chron C3An.1n (Supplementary 1). Such behaviour, interpreted as delayed acquisition, is typical for different generations of greigite and was previously also described for chron C3r in the Bădislava section in the Dacian Basin (Vasiliev et al., 2008). The exact position of the C3An.1n–C3r polarity boundary in the Rîmnicu Sărat section is thus uncertain, which might explain the small age difference with other Eastern Paratethys sections. Our high-resolution palaeomagnetic age constraint resolves this discrepancy and confirms a 6.1 Ma age for the Maeotian – Pontian boundary in the Dacian Basin, in analogy with the Caspian and Black Sea Basins (van Baak et al., 2016; Rostovtseva and Rybkina, 2017).

The age of the Khersonian–Maeotian boundary has long been uncertain, with attributed ages differing as much as 3 Myr: 10.5 Ma (Matenco et al., 2003), 9.3 Ma (Nevesskaya et al., 2003), 7.6 Ma (Trubikhin, 1989). Recent studies, however, seem to have solved this controversy. In the Black Sea, the Khersonian–Maeotian boundary was magneto- and cyclostratigraphically dated at 7.6 Ma (Rybkina et al., 2015). In the Dacian Basin, initiation of the Maeotian transgression was dated at 7.65 Ma (slightly below C4n.1n–C4n.1r polarity reversal) (Palcu et al., 2019b).

There are two possible options for correlation of our normal zone N1. The most likely correlation, in our opinion, would be to chron C4n.1n, which would be in accordance with a Khersonian-Maeotian boundary near 7.6 or 7.65 Ma (Option 1). An alternative is to correlate to chron C3Bn (Option 2), or any of the other normal chrons between C3Bn and C4n.1n (Fig. 14). Option 1 results in a sedimentation rate of 0.78 m/kyr, subsequently gently decreasing to 0.67 m/kyr and 0.65 m/kyr (Fig. 14). Option 2 results in an initial sedimentation rate of 1.23 m/kyr with a subsequent decrease down to 1.05 m/kyr and then to 0.65 m/kyr. Correlation to chron C4n.1n (Option 1) does not lead to any severe changes of sedimentation rates. The remainder of normal chron C3An.2n would completely fall in the unexposed interval between 734 and 916 m and C3Bn as well as C3Br.1n would fall in the unexposed interval between 370 m and 601 m. We prefer to correlate N1 to C4n.1n (Option 1), which results in a 7.63 ± 0.05 Ma age for the Maeotian – Khersonian boundary (150.8 m) in the Slănicul de Buzău section, in close accordance with previous results.

5.2. Palaeoenvironmental reconstruction from Slănicul de Buzău and its relation with the evolution of the Eastern Paratethys

5.2.1. Coastal plain deposition during the late Khersonian

During the Khersonian, climate in the Eastern Paratethys region became more arid, and open steppe-like landscapes dominated, where a xerophytic-type vegetation developed (Ivanov et al., 2011). This period, also known as the Khersonian drying, provoked a disruption of the sensitive water budget that resulted in high-amplitude water-level fluctuations (Popov et al., 2010; Ivanov et al., 2011; Palcu et al., 2019b). The facies trend in the Slănicul de Buzău section reflects two intervals (0–62.2 m and 127.5–150.8) with well-developed palaeosols separated by an interval with littoral (offshore-shoreface) facies (Fig. 15). Stratigraphically, this interval corresponds to the uppermost Khersonian lake-level lowstand indicated by Popov et al. (2006).The *Chersonimactra bulgarica* biozone spans the upper Khersonian (Kojumdgieva et al., 1989). The indicative species, *Chersonimactra bulgarica* and *Ch. caspia* are widely distributed in our section within the first red interval and in the subsequent interval with littoral deposits (Fig. 15).

5.2.2. Early Maeotian transgression and establishment of a littoral environment

The great Khersonian drying was terminated by the widely recognized Maeotian transgression that was caused by a climatically-driven switch to an overall positive hydrological balance of the Eastern Paratethys (Palcu et al., 2019b). At the onset of the Maeotian, the depositional environment in the Slănicul de Buzău area suddenly changed from a coastal plain, characteristic for the Khersonian (SI1), to an offshore setting (SI2). The offshore interval (SI2) contains abundant *Ammonia beccarii*, an event that is also characteristic for the lowermost Maeotian in other parts of the Eastern Paratethys and is known as the "*Ammonia* acme zone" (Popescu, 1995; Pinchuk, 2006). In the neighbouring Euxinian Basin this zone is taxonomically richer and also contains numerous species of the *Quinqueloculina* and *Cassidulina* genera as well as abundant *Tamanicella lapidosa* bryozoa (Popov et al., 2016), which indicate a higher salinity. The salinity, based on the coexistence of certain microfauna groups in the entire lower Maeotian of the Euxinian Sea (Taman Peninsula) is estimated between 7 and 13‰ (Popov et al., 2016), while we estimate salinity for the lowermost Maeotian offshore interval (SI2) along Slănicul de Buzău between 6 and 10‰ (low mesohaline), and for the rest of the lower Maeotian (SI3) between 3 and 5‰ (oligohaline) (Fig. 15). The post-flooding lower Maeotian comprises alternating offshore, shoreface, barrier and back-barrier lagoon deposits, reflecting shallower environment than the Maeotian flooding ofsshore settings. This shallowing trend, however, turned back to deepening again just before the gap in exposure (370–600 m, Fig. 4). After the gap, the upper part of SI3 has sedimentary facies more characteristic for somewhat deeper settings as it is dominated by offshore transition and offshore facies.

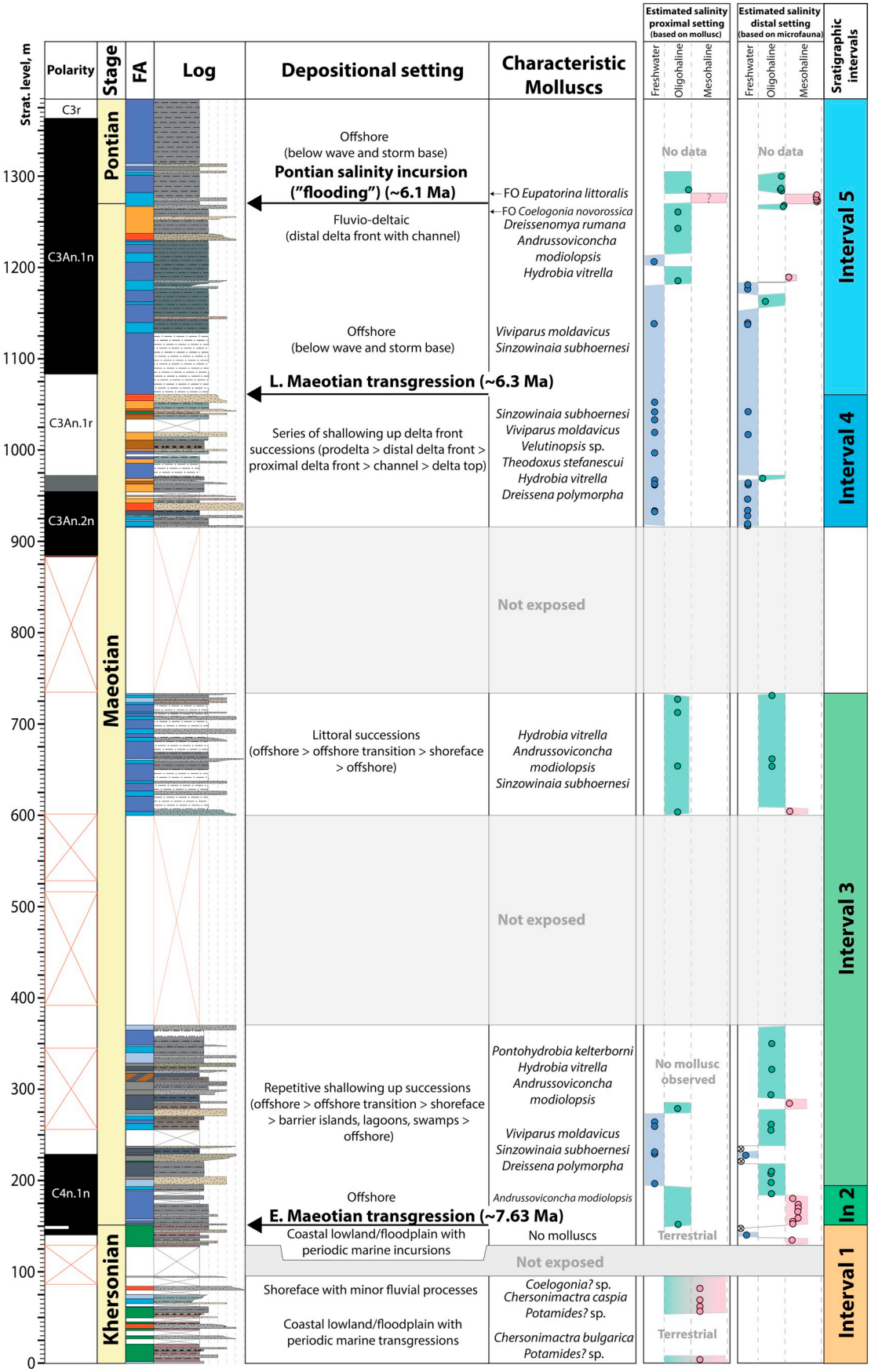

Fig. 15. Reconstruction of the palaeoenvironmental evolution along the Slănicul de Buzău section during the Khersonian–Maeotian with characteristic depositional environments, mollusc fauna and estimated salinity in proximal and distal setting. The colour meaning in the facies association column is shown in the legend of Fig. 4.

5.2.3. Deposition at the mouth of the Balta Delta in the late Maeotian

The upper Maeotian (SI4) of Slănicul de Buzău is characterized by delta-front cyclicity and a prevalence of freshwater microfauna in both delta-front and prodelta depositional settings. The littoral environments that dominate the lower Maeotian (SI3) indicate that, at that time, our study area was located along the shore, but not at the mouth of a major delta. The delta front became located in the Slănicul de Buzau area from ~6.5–6.3 Ma, likely due to progradation of the Balta Delta along the axis of the East Carpathian Foreland (Matoshko et al., 2016; De Leeuw et al., 2020). This indicates that sediment supply outpaced the creation of accommodation space, reflecting a change in the balance of subsidence, sea-level and sediment supply. Whereas hummocky cross stratification and the frequent occurrence of wave ripples indicate significant wave influence in the lower Meotian (SI3), the delta-front deposits of SI4 lack distinctive wave structures. This is similar to the conclusion of Jorissen et al. (2018), regarding the lack of wave influence in the deltaic deposits of the Dacian interval of the Slănicul de Buzău Section. The delta-front cycles in SI4 resemble those of the Dacian interval and are thus interpreted to be river dominated.

The domination of freshwater fauna in SI4 is quite striking (Fig. 15). Freshwater fauna furthermore dominates the thick offshore deposits of the directly overlying lower part of SI5 (see below). Low brackish microfauna occur only very occasionally in the most distal settings of SI4 and the lower part of SI5 (Fig. 15). This distinctive freshening of the Dacian Basin in the late Meotian points at a restricted connection with the brackish Euxinian Basin (Popov et al., 2016) and a strong control of the basinal water budget by riverine fresh water input. This may have been caused by the progradation of the Balta Delta (De Leeuw et al., 2020): Sediment supplied by this delta may have narrowed or closed the gateway between the Dacian Basin and the Euxinian Basin leading to restriction and subsequent freshening of the Dacian Basin.

5.2.4. Latest Maeotian freshwater transgression and early Pontian "flooding"

The shallow-water deltaic deposits of SI4 are overlain by a thick succession of offshore mudstones (SI5), indicating a major rise in base-level (Fig. 15). This event, which we interpret as a major transgression, started at 6.3 Ma (correlated to C3An.1r), with maximum water levels reached in the early Pontian for which high water-levels are known from all around the Eastern Paratethys (Popov et al., 2006, 2010). The offshore deposits of the lower part of SI5 contain freshwater molluscs and microfauna, meaning the Dacian Basin remained fresh during the initial transgression (Fig. 15). The contemporaneous fossil record of the neighbouring Euxinian Basin, on the other hand, contains brackish water fauna (Popov et al., 2016). This difference in the faunal assemblages of the two basins indicates that, at least during the early part of the transgression, freshwater input to the Dacian Basin and its restriction from the Euxinian Basin were sufficient enough to keep the basin's water fresh.

The late Maeotian transgression appears to go along with a remarkable increase in sedimentation rate from 0.65 m/kyr within C3An.1r chron to 1.26 m/kyr within C3An.1n (Fig. 14). The Slănicul de Buzău section is located on the western flank of the Focşani Depression – a depocentre that experienced enhanced subsidence during the latest Miocene–Pliocene (Leever, 2007; Panaiotu et al., 2007) as expressed in a markedly thicker depositional record compared to the western Dacian Basin (Jipa and Olariu, 2009). Around the Focşani Depression, a similar increase of sedimentation rate from 0.6 m/kyr to 1.5 m/kyr was previously detected within the C3r chron (Pontian) along the Putna and Râmnicu Sărat sections (Vasiliev et al., 2004; Panaiotu et al., 2007). The Bizdidel section, which is located more to the west, outside the Focşani Depression, shows a sediment accumulation rate of only 0.3 m/kyr within the C3An.1n chron (Snel et al., 2006): Almost five times lower than at Slănicul de Buzau. This increase of sedimentation rates and the concurrent deepening of the depositional environment that we register along Slănicul de Buzău were likely linked to an amplification of subsidence in the Focşani Depression, which rapidly augmented accommodation space.

Higher up in the section, from 1166 m upwards, we discovered the first influxes of brackish water microfauna (Fig. 6) and molluscs (Tables 2, 1186.6 m), which initially alternate with freshwater taxa. The presence of *Typhlocyprella* sp. indicates the first pulses of brackish water from Lake Pannon. Modelling of the connection between Lake Pannon and the Dacian Basin suggests at least a one-way flow from the upstream Lake Pannon to the Dacian Basin at the Maeotian–Pontian transition (Leever, 2007). The one-way flow is also supported by the absence of Eastern Paratethyan faunistic groups in Lake Pannon at that time (Magyar et al., 1999).

At 1265 m, the occurrence of *Coelogonia novorossica* preludes the Maeotian–Pontian transition (Roshka, 1973; Stoica et al., 2007; Stoica et al., 2016). At 1270 m, an abundant meso-polyhaline fauna assemblage with the foraminifera *Ammonia*, *Porosononion* and *Quinqueloculina* and *Streptochilus* occurs. This short influx of "marine" microfauna at 6.1 Ma (Figs. 11, 15) is known as the "Pontian flooding" and has been traced in all parts of the Eastern Paratethys: in the Dacian Basin (Stoica et al., 2013), the Euxinian Basin (Taman Peninsula- Zhelezniy Rog section) (Krijgsman et al., 2010), Western Caucasus (Maissuradze, 1988) and Azerbaijan (van Baak et al., 2016). Occurrence of this assemblage is linked to the establishment of a short connection between the Mediterranean, Eastern Paratethys and possibly Lake Pannon (Krijgsman et al., 2010; Stoica et al., 2013). Given that our results along Slănicul de Buzău indicate that the transgressive systems tract started at 6.3 Ma, well before the appearance of foraminifera at 6.1 Ma, it would in our opinion be better to change the name of the foraminifera level from "Pontian Flooding" into "Pontian Salinity Incursion".

The interval with foraminifera is shortly followed (at 1279 m) by the appearance of typical early Pontian oligohaline molluscs and ostracods: *Pontoniella acuminata, Candona (Hastacandona) lotzy, Candona (Hastacandona) hysterica, Candona (Zalaniella) venusta* etc. (Fig. 11). This fauna, which originated in Lake Pannon, used the Dacian Basin as a springboard to spread all over the Eastern Paratethys at the onset of the Pontian (Stevanovic et al., 1989; Popov et al., 2006; Grothe et al., 2018), and eventually entered the Mediterranean Basin in the latest Messinian (Taviani et al., 2007; Stoica et al., 2016). The first occurrence of molluscs that biostratigraphically defines the early Pontian is situated 9 m above the "Pontian Salinity Incursion" that, considering the high sedimentation rate, means a delay of ~6 kyr. We choose to place the chronostratigraphic base of the Pontian at the foraminifera bearing level corresponding to an age of 6.1 Ma.

6. Conclusions

Our integrated magneto-biostratigraphy, with observations of sedimentary facies and fossil fauna distribution, contributes to a better understanding of the palaeoenvironmental evolution of the Dacian Basin during the late Miocene (late Khersonian–early Pontian) interval. In the uppermost Khersonian we observed a low relative water level marked by the development of red palaeosols shortly interrupted by an interval with offshore- shoreface environments. A monospecific Khersonian mollusc assemblage with *Chersonimactra bulgarica* is widely present, but disappears in the upper palaeosol interval. The Khersonian was terminated by the Maeotian transgression that is correlated here to Chron C4n.1n and dated at ~7.63 Ma. The transgressive interval contains abundant *Ammonia beccarii* foraminifera and brackish water ostracods. The early Maeotian comprises shoreface, barrier and back-barrierlagoon environments. The presence of freshwater molluscs in shallow water facies such as shoreface and barrier islands, and oligohaline microfauna in deeper-water facies indicative of offshore to offshore transition environments suggests that the deeper basin remained brackish, whereas marginal environments felt a distinctive freshwater influence. In the late Maeotian (6.5–6.3 Ma), the area was characterized by delta-front deposition with abundant freshwater molluscs and

freshwater microfauna. An abrupt replacement of deltaic deposits by relatively deep water offshore ones subsequently provides evidence for a major transgression that started in the late Maeotian at 6.3 Ma. Several pulses with brackish water microfauna with *Typhlocyprella* sp. follow the initial rise in base level and suggest a periodic overflow of Lake Pannon into the Dacian Basin. The Maeotian–Pontian boundary is marked by a short-duration influx of a meso- polyhaline microfaunal assemblage dominated by planktonic and benthic foraminifera. This event is commonly known as the "Pontian Flooding" but might better be named "Pontian Salinity Incursion" given that the transgression started in the late Maeotian. Our high-resolution magneto-biostratigraphic dating places the Pontian Salinity Incursion at ~6.1 Ma and indicates that it was synchronous throughout the entire Eastern Paratethys. The typical Pontian mollusc and ostracod assemblages first appear 9 m above the salinity incursion.

Our palaeoenvironmental reconstruction highlights the importance of an integrative approach. Simultaneous analyses of sedimentary facies, micro- and macrofauna allows to better constrain where in the depositional environment particular organisms were present, which leads to an improved understanding of the evolution of salinity in the basin and along its margin. This approach is particularly important in semi-isolated marginal basins like the Eastern Paratethys and the Dacian Basin, which combine features of marine basins as well as freshwater lakes.

Supplementary data to this article can be found online at https://doi.org/10.1016/j.gloplacha.2020.103224.

Declaration of Competing Interest

None.

Acknowledgments

We thank our colleagues from CASP and Paleomagnetic laboratory "Fort Hoofddijk" for scientific support and advice during the writing of this paper. We also thank Pierre Polard-Taine for help with the palaeomagnetic measurements and Alberto Martínez Gándara and Gülçin Aygün for assistance in the field. We would also like to give special thanks to editor Prof. Dr. Liviu Matenco and to Dr. Sergey Popov (GIN RAS, Moscow) and two other anonymous reviewers for valuable comments that allowed to significantly improve the manuscript. This research is part of the PRIDE project (Pontocaspian RIse and DEmise), which was funded by the European Union's Horizon 2020 research and innovation program, under the Marie Skłodowska-Curie Action (grant agreement № 642973).

References

Allen, J.L., Johnson, C.L., 2011. Architecture and formation of transgressive-regressive cycles in marginal marine strata of the John Henry Member, Straight Cliffs Formation, Upper cretaceous of Southern Utah, USA. Sedimentology 58, 1486–1513. https://doi.org/10.1111/j.1365-3091.2010.01223.x.

Amorosi, A., Centineo, M.C., Colalongo, M.L., Pasini, G., Sarti, G., Vaiani, S.C., 2003. Facies Architecture and latest Pleistocene–Holocene Depositional history of the Po Delta (Comacchio Area), Italy. J. Geol. 111, 39–56. https://doi.org/10.1086/344577.

Amorosi, A., Maselli, V., Trincardi, F., 2016. Onshore to offshore anatomy of a late Quaternary source-to-sink system (Po Plain–Adriatic Sea, Italy). Earth Sci. Rev. 153, 212–237. https://doi.org/10.1016/j.earscirev.2015.10.010.

Andrusov, N.I., 2015. Kerchenskiy izvestnyak i ego fauna: (c 5-yu tablitsami). Zapiski Imp. mineralogicheskogo obshchestva 26, 193–344 Saint Petersburg. (In Russian).

Ashley, G.M., Southard, J.B., Boothroyd, J.C.O.N., 1982. Deposition of climbing-ripple beds: a flume simulation. Sedimentology 29, 67–79. https://doi.org/10.1111/j.1365-3091.1982.tb01709.x.

Bann, K.L., Fielding, C.R., Maceachern, J.A., Tye, S.C., 1977. Differentiation of estuarine and offshore marine deposits using integrated ichnology and sedimentology: Permian Pebbley Beach Formation, Sydney Basin, Australia. In: McIlroy, D. (Ed.), The Application of Ichnology to Palaeoenvironmental and Stratigraphic Analysis: Geological Society of London. Special Publication, pp. 179–211 GSL.SP.2004.228.01.10.

Bhattacharya, J.P., MacEachern, J.A., 2009. Hyperpycnal rivers and prodeltaic shelves in the cretaceous seaway of North America. J. Sediment. Res. 79, 184–209. https://doi.org/10.2110/jsr.2009.026.

Buatois, L.A., Santiago, N., Herrera, M., Plink-Björklund, P., Steel, R.O.N., Espin, M., Parra, K., 2012. Sedimentological and ichnological signatures of changes in wave, river and tidal influence along a Neogene tropical deltaic shoreline. Sedimentology 59, 1568–1612. https://doi.org/10.1111/j.1365-3091.2011.01317.x.

Chang, L., Vasiliev, I., van Baak, C., Krijgsman, W., Dekkers, M.J., Roberts, A.P., Gerald, J.D.F., van Hoesel, A., Winklhofer, M., 2014. Identification and environmental interpretation of diagenetic and biogenic greigite in sediments: a lesson from the Messinian Black Sea. Geochem. Geophys. Geosyst. 15, 3612–3627. https://doi.org/10.1002/2014GC005411.

Cheel, R., 1978. Hummocky and swaley cross-stratification. In: Sedimentology. Springer Berlin Heidelberg, pp. 585–588.

Chentnik, B.M., Johnson, C.L., Mulhern, J.S., Stright, L., 2015. Valleys, estuaries, and lagoons: paleoenvironments and regressive–transgressive architecture of the upper cretaceous straight cliffs formation, Utah, U.S.A. J. Sediment. Res. 85, 1166–1196. https://doi.org/10.2110/jsr.2015.70.

Collinson, J.D., 1969. The sedimentology of the grindslow shales and the kinderscout grit: a deltaic complex in the namurian of Northern England. J. Sed. Res. 39. https://doi.org/10.1306/74D71C17-2B21-11D7-8648000102C1865D.

Cronin, B., Owen, D., Hartley, A., Kneller, B., 1998. Slumps, debris flows and sandy deep-water channel systems: implications for the application of sequence stratigraphy to deep water clastic sediments. J. Geol. Soc. 155, 429–432. https://doi.org/10.1144/gsjgs.155.3.0429.

De Leeuw, A., Bukowski, K., Krijgsman, W., Kuiper, K.F., 2010. Age of the Badenian salinity crisis; impact of Miocene climate variability on the circum-Mediterranean region. Geol 38, 715–718. https://doi.org/10.1130/G30982.1.

De Leeuw, A., Tulbure, M., Kuiper, K.F., Melinte-Dobrinescu, M.C., Stoica, M., Krijgsman, W., 2018. New 40Ar/39Ar, magnetostratigraphic and biostratigraphic constraints on the termination of the Badenian Salinity Crisis: Indications for tectonic improvement of basin interconnectivity in Southern Europe. Glob. Planet. Chang. 169, 1–15. https://doi.org/10.1016/j.gloplacha.2018.07.001.

De Leeuw, A., Vincent, S.J., Matoshko, A., Stoica, M., Igorara, I., 2020. Late Miocene sediment delivery from the axial drainage system of the East Carpathian foreland basin to the Black Sea. Geology 48. https://doi.org/10.1130/G47318.1.

Dott, R.H., Bourgeois, J., 1982. Hummocky stratification: significance of its variable bedding sequences. Geol. Soc. Am. Bull. 93, 663. https://doi.org/10.1130/0016-7606(1982)93<663:HSSOIV>2.0.CO;2.

Dumitrescu, I., Sandulescu, M., Bandrabur, T., 1970. Geologic Map of Romania: Covasna Sheet.

Dupont-Nivet, G., Vasiliev, I., Langereis, C.G., Krijgsman, W., Panaiotu, C., 2005. Neogene tectonic evolution of the southern and eastern Carpathians constrained by paleomagnetism. Earth Planet. Sci. Lett. 236, 374–387. https://doi.org/10.1016/j.epsl.2005.04.030.

Fielding, C.R., 2010. Planform and Facies Variability in Asymmetric Deltas: Facies Analysis and Depositional Architecture of the Turonian Ferron Sandstone in the Western Henry Mountains, South-Central Utah, U.S.A. J. Sediment. Res. 80, 455–479. https://doi.org/10.2110/jsr.2010.047.

Flügel, E., 2010. Microfacies of Carbonate Rocks: Analysis, Interpretation and Application, 2nd ed. Springer-Verlag Berlin Heidelberg, Berlin, Heidelberg (984 pp).

Forzoni, A., Hampson, G., Storms, J., 2015. Along-strike variations in stratigraphic architecture of shallow-marine reservoir analogues: upper cretaceous panther tongue delta and coeval shoreface, star point sandstone, Wasatch Plateau, Central Utah, U.S.A. J. Sediment. Res. 85, 968–989. https://doi.org/10.2110/jsr.2015.69.

Gérard, J.R.F., Bromley, R.G., 2008. Ichnofabrics in Clastic Sediments: a Practical Guide. Association des Sédimentologistes Français, [Place of Publication Not Identified]. (100 pp).

Gillet, H., Lericolais, G., Réhault, J.-P., 2007. Messinian event in the Black Sea: evidence of a Messinian erosional surface. Mar. Geol. 244, 142–165. https://doi.org/10.1016/j.margeo.2007.06.004.

Golovina, L.A., Radionova, E.P., van Baak, C.G.C., Krijgsman, W., Palcu, D.V., 2019. A late Maeotian age (6.7–6.3 Ma) for the enigmatic "Pebbly Breccia" unit in DSDP Hole 380A of the Black Sea. Palaeogeogr. Palaeoclimatol. Palaeoecol. 109269. https://doi.org/10.1016/j.palaeo.2019.109269.

Grothe, A., 2016. The Messinian Salinity Crisis: A Paratethyan Perspective: De Messiniaanse Zoutcrisis: Een Paratethys' Perspectief. Ridderprint BV, Ridderkerk (151 pp).

Grothe, A., Sangiorgi, F., Brinkhuis, H., Stoica, M., Krijgsman, W., 2018. Migration of the dinoflagellate *Galeacysta etrusca* and its implications for the Messinian Salinity Crisis. Newsl. Stratigr. 51, 73–91. https://doi.org/10.1127/nos/2016/0340.

Grothe, A., Andreetto, F., Reichart, G.-J., Wolthers, M., van Baak, C.G.C., Vasiliev, I., Stoica, M., Sangiorgi, F., Middelburg, J.J., Davies, G.R., Krijgsman, W., 2020. Paratethys pacing of the Messinian Salinity Crisis: Low salinity waters contributing to gypsum precipitation? Earth Planet. Sci. Lett. 532, 116029. https://doi.org/10.1016/j.epsl.2019.116029.

Hampson, G.J., Sixsmith, P.J., Kieft, R.L., Jackson, C.A.-L., Johnson, H.D., 2009. Quantitative analysis of net-transgressive shoreline trajectories and stratigraphic architectures: mid-to-late Jurassic of the North Sea rift basin. Basin Res. 21, 528–558. https://doi.org/10.1111/j.1365-2117.2009.00414.x.

Hayes, M.O., FitzGerald, D.M., 2013. Origin, evolution, and classification of tidal inlets. J. Coast. Res. 69, 14–33. https://doi.org/10.2112/SI_69_3.

Hilgen, F.J., Lourens, L.J., van Dam, J.A., Beu, A.G., Boyes, A.F., Cooper, R.A., Krijgsman, W., Ogg, J.G., Piller, W.E., Wilson, D.S., 2012. The Neogene period. In: The Geologic Time Scale. Elsevier, pp. 923–978.

Iljina, L.A., Nevesskaja, L.A., Paramonova, N.P., 1976. Regularities of Mollusc Development in the Neogene Semimarine and Brackishwater Basins of Eurasia (Late Miocene - Early Pliocene). Publishing House "Nauka", Moscow.

Ivanov, D., Utescher, T., Mosbrugger, V., Syabryaj, S., Djordjević-Milutinović, D., Molchanoff, S., 2011. Miocene vegetation and climate dynamics in Eastern and Central Paratethys (Southeastern Europe). Palaeogeogr. Palaeoclimatol. Palaeoecol. 304, 262–275. https://doi.org/10.1016/j.palaeo.2010.07.006.

Jipa, D., Olariu, C., 2009. Dacian Basin: Depositional Architecture and Sedimentary

History of a Paratethys Sea. GeoEcoMar, Bucharest (264 pp).
Jorissen, E.L., de Leeuw, A., van Baak, C.G.C., Mandic, O., Stoica, M., Abels, H.A., Krijgsman, W., 2018. Sedimentary architecture and depositional controls of a Pliocene river-dominated delta in the semi-isolated Dacian Basin, Black Sea. Sediment. Geol. 368, 1–23. https://doi.org/10.1016/j.sedgeo.2018.03.001.
Jorissen, E., Abels, H., Wesselingh, F., Lazarev, S., Aghayeva, V., Krijgsman, W., 2019. Amplitude, frequency and drivers of Caspian Sea lake-level variations during the early Pleistocene and their impact on a protected wave-dominated coastline. Sedimentology. https://doi.org/10.1111/sed.12658.
Karami, M.P., De Leeuw, A., Krijgsman, W., Meijer, P.T., Wortel, M.T.R., 2011. The role of gateways in the evolution of temperature and salinity of semi-enclosed basins: An oceanic box model for the miocene mediterranean sea and paratethys. Glob. Planet. Chang. 79, 73–88. https://doi.org/10.1016/j.gloplacha.2011.07.011.
Kelder, N.A., Sant, K., Dekkers, M.J., Magyar, I., van Dijk, G.A., Lathouwers, Y.Z., Sztanó, O., Krijgsman, W., 2018. Paleomagnetism in Lake Pannon: problems, pitfalls, and progress in using iron sulfides for magnetostratigraphy. Geochem. Geophys. Geosyst. 19, 3405–3429. https://doi.org/10.1029/2018GC007673.
Kieft, R.L., Jackson, C.A.-L., Hampson, G.J., Larsen, E., 2010. Sedimentology and sequence stratigraphy of the Hugin Formation, Quadrant 15, Norwegian sector, South Viking Graben. Pet. Geol. Conf. Ser. 7, 157–176. https://doi.org/10.1144/0070157.
Kieft, R.L., Hampson, G.J., Jackson, C.A.-L., Larsen, E., 2011. Stratigraphic architecture of a net-transgressive marginal- to shallow-marine succession: upper almond formation, Rock Springs Uplift, Wyoming, U.S.A. J. Sediment. Res. 81, 513–533. https://doi.org/10.2110/jsr.2011.44.
Kojumdgieva, E.I., 1969. Fosilite na Bulgaria VIII Sarmat., Sofija.
Kojumdgieva, E.I., Paramonova, N.P., Belokrys, K.S., Muskhelishvili, L.V., 1989. Ecostratigraphic subdivision of the Sarmatian after molluscs. Gologica Carpathica 40, 81–84.
Koymans, M.R., Langereis, C.G., Pastor-Galan, D., Hinsbergen, D.J.J., 2016. Paleomagnetism.org: an online multi-platform open source environment for paleomagnetic data analysis. Comput. Geosci. 93, 127–137.
Kraus, M.J., 1999. Paleosols in clastic sedimentary rocks: their geologic applications. Earth Sci. Rev. 47, 41–70. https://doi.org/10.1016/S0012-8252(99)00026-4.
Krijgsman, W., Stoica, M., Vasiliev, I., Popov, V.V., 2010. Rise and fall of the Paratethys Sea during the Messinian Salinity Crisis. Earth Planet. Sci. Lett. 290, 183–191. https://doi.org/10.1016/j.epsl.2009.12.020.
La de Vara, A., van Baak, C.G.C., Marzocchi, A., Grothe, A., Meijer, P.T., 2016. Quantitative analysis of Paratethys Sea level change during the Messinian Salinity Crisis. Mar. Geol. 379, 39–51. https://doi.org/10.1016/j.margeo.2016.05.002.
Laskarev, V., 1924. Sur les equivalentes du Sarmatien supérieur en Serbie. Recueil de traveaux ofert a M. Jovan Cvijic par ses amis et collaborateurs 73–85.
Leever, K.A., 2007. Foreland of the Romanian Carpathians: Controls on Late Orogenic Sedimentary Basin Evolution and Paratethys Paleogeography. [s.n.], [S.l.], XIV, 182.
Leever, K.A., Matenco, L., Rabagia, T., Cloetingh, S., Krijgsman, W., Stoica, M., 2010. Messinian Sea level fall in the Dacic Basin (Eastern Paratethys): palaeogeographical implications from seismic sequence stratigraphy. Terra Nova 22, 12–17. https://doi.org/10.1111/j.1365-3121.2009.00910.x.
The venice system for the classification of marine waters according to salinity. Limnol. Oceanogr. 3, 346–347. https://doi.org/10.4319/lo.1958.3.3.0346.
MacEachern, J.A., Bann, K.L., 2008. The role of ichnology in refining shallow marine facies models. In: Hampson, G.J., Steel, R.J., Burgess, P.M., Dalrymple, R.W. (Eds.), Recent Advances in Models of Siliciclastic Shallow-Marine Stratigraphy. SEPM (Society for Sedimentary Geology), pp. 73–116.
MacEachern, J., Bann, K., Bhattacharya, J., Howell Jr., C., 2005. Ichnology of Deltas: Organism responses to the dynamic interplay of rivers, waves, storms and tides. In: River Deltas-Concepts, Models, and Examples. 83 SPEM Special Publication.
Magyar, I., Geary, D.H., Müller, P., 1999. Paleogeographic evolution of the late Miocene Lake Pannon in Central Europe. Palaeogeogr. Palaeoclimatol. Palaeoecol. 147, 151–167. https://doi.org/10.1016/S0031-0182(98)00155-2.
Maisuradze, L.S., 1988. Foraminifera of the Meotian of Western Georgia. Metzniereba, pp. 73.
Mandic, O., Sant, K., Kallanxhi, M.-E., Ćorić, S., Theobalt, D., Grunert, P., de Leeuw, A., Krijgsman, W., 2019. Integrated bio-magnetostratigraphy of the Badenian reference section Ugljevik in southern Pannonian Basin - implications for the Paratethys history (middle Miocene, Central Europe). Glob. Planet. Chang. 172, 374–395. https://doi.org/10.1016/j.gloplacha.2018.10.010.
Marzocchi, A., Flecker, R., van Baak, C.G.C., Lunt, D.J., Krijgsman, W., 2016. Mediterranean outflow pump: an alternative mechanism for the Lago-mare and the end of the Messinian Salinity Crisis. Geology 44, 523–526. https://doi.org/10.1130/G37646.1.
Matenco, L., Bertotti, G., Cloetingh, S., Dinu, C., 2003. Subsidence analysis and tectonic evolution of the external Carpathian–Moesian Platform region during Neogene times. Sediment. Geol. 156, 71–94. https://doi.org/10.1016/S0037-0738(02)00283-X.
Matoshko, A., Matoshko, A., de Leeuw, A., Stoica, M., 2016. Facies analysis of the balta formation: evidence for a large late Miocene fluvio-deltaic system in the East Carpathian Foreland. Sediment. Geol. 343, 165–189. https://doi.org/10.1016/j.sedgeo.2016.08.004.
Matoshko, A., Matoshko, A., de Leeuw, A., 2019. The plio–pleistocene demise of the East Carpathian Foreland Fluvial system and arrival of the Paleo-Danube to the Black Sea. Geol. Carpath. 70, 91–112. https://doi.org/10.2478/geoca-2019-0006.
McCubbin, D.G., 1982. Barrier-Island and strand plain facies. In: Horn, M.K. (Ed.), Sandstone Depositional Environments, pp. 247–281.
McFadden, P.L., McElhinny, M.W., 1990. Classification of the reversal test in palaeomagnetism. Geophys. J. Int. 103, 725–729. https://doi.org/10.1111/j.1365-246X.1990.tb05683.x.
Miall, A.D., 1996. The Geology of Fluvial Deposits: Sedimentary Facies, Basin Analysis, and Petroleum Geology / Andrew D. Miall. Springer, Berlin, London.
Motas, I., Bandrabur, T., Ghenea, C., Sandulescu, M., 1966. Geologic Map of Romania: Ploiesti Sheet.
Mulder, T., Syvitski, J.P.M., Migeon, S., Faugères, J.-C., Savoye, B., 2003. Marine hyperpycnal flows: initiation, behavior and related deposits. A review. Mar. Pet. Geol. 20, 861–882. https://doi.org/10.1016/j.marpetgeo.2003.01.003.
Mullender, T.A.T., Velzen, A.J., Dekkers, M.J., 1993. Continuous drift correction and separate identification of ferrimagnetic and paramagnetic contributions in thermomagnetic runs. Geophys. J. Int. 114, 663–672. https://doi.org/10.1111/j.1365-246X.1993.tb06995.x.
Mullender, T.A.T., Frederichs, T., Hilgenfeldt, C., de Groot, L.V., Fabian, K., Dekkers, M.J., 2016. Automated paleomagnetic and rock magnetic data acquisition with an inline horizontal “2G” system. Geochem. Geophys. Geosyst. 17, 3546–3559. https://doi.org/10.1002/2016GC006436.
Nadon, G.C., Issler, D.R., 1997. The compaction of floodplain sediments: timing, magnitude and implications. Geosci. Can. 21, 38–42.
Nevesskaja, L.A., Goncharova, I.A., Paramonova, N.P., Popov, S.B., Babak, E.B., Bagdasarjan, K.G., Voronina, A.A., 1993. Opredelitelj miocenovjih dvustvorchatjih molljuskov Jugo-Zapadnoi Evrazii. Nauka, Moscow (412 pp).
Nevesskaja, L.A., Paramonova, N.P., Babak, E.V., 1997. Opredelitel pliocenovih dvustvorchatih molluskov Jugozapadnoj Evrazii. Trudi Paleontologičeskogo Instituta 269, 1–220.
Nevesskaya, L.A., Goncharova, I.A., Ilyina, L.B., Paramonova, N.P., Khondkarian, S.O., 2003. The Neogene stratigraphic scale of the Eastern Paratethys. Stratigr. Geol. Correl. 11, 105–127.
Nevesskaya, L.A., Popov, S.V., Goncharova, I.A., Guzhov, A.V., Yanin, B.T., Polubotko, I.V., Biakov, A.S., Gavrilova, V.A., 2013. Phanerozoic Bivalvia of Russia and adjacent countries. Tr. Paleontol. Inst. Ross. Akad. Nauk 294, 1–524.
Oliveira, C.M.M., Hodgson, D.M., Flint, S.S., 2009. Aseismic controls on in situ soft-sediment deformation processes and products in submarine slope deposits of the Karoo Basin, South Africa. Sedimentology 56, 1201–1225. https://doi.org/10.1111/j.1365-3091.2008.01029.x.
Oliveira, C.M.M., Hodgson, D.M., Flint, S.S., 2011. Distribution of soft-sediment deformation structures in clinoform successions of the Permian Ecca Group, Karoo Basin, South Africa. Sediment. Geol. 235, 314–330. https://doi.org/10.1016/j.sedgeo.2010.09.011.
Opluštil, S., Lojka, R., Rosenau, N.A., Strnad, L., Sýkorová, I., 2015. Middle Moscovian climate of eastern equatorial Pangea recorded in paleosols and fluvial architecture. Palaeogeogr. Palaeoclimatol. Palaeoecol. 440, 328–352. https://doi.org/10.1016/j.palaeo.2015.09.009.
Palcu, D.V., Tulbure, M., Bartol, M., Kouwenhoven, T.J., Krijgsman, W., 2015. The Badenian–Sarmatian Extinction Event in the Carpathian foredeep basin of Romania: Paleogeographic changes in the Paratethys domain. Glob. Planet. Chang. 133, 346–358. https://doi.org/10.1016/j.gloplacha.2015.08.014.
Palcu, D.V., Golovina, L.A., Vernyhorova, Y.V., Popov, S.V., Krijgsman, W., 2017. Middle Miocene paleoenvironmental crises in Central Eurasia caused by changes in marine gateway configuration. Glob. Planet. Chang. 158, 57–71. https://doi.org/10.1016/j.gloplacha.2017.09.013.
Palcu, D.V., Popov, S.V., Golovina, L.A., Kuiper, K.F., Liu, S., Krijgsman, W., 2019a. The shutdown of an anoxic giant: Magnetostratigraphic dating of the end of the Maikop Sea. Gondwana Res. 67, 82–100. https://doi.org/10.1016/j.gr.2018.09.011.
Palcu, D.V., Vasiliev, I., Stoica, M., Krijgsman, W., 2019b. The end of the Great Khersonian Drying of Eurasia: Magnetostratigraphic dating of the Maeotian transgression in the Eastern Paratethys. Basin Res. 31, 33–58. https://doi.org/10.1111/bre.12307.
Panaiotu, C.E., Vasiliev, I., Panaiotu, C.G., Krijgsman, W., Langereis, C.G., 2007. Provenance analysis as a key to orogenic exhumation: a case study from the East Carpathians (Romania). Terra Nova 19, 120–126. https://doi.org/10.1111/j.1365-3121.2006.00726.x.
Paramonova, N.P., 1994. History of Sarmatian and Akchagylian Bivalves. Nauka, Moscow.
Piller, W.E., Harzhauser, M., Mandic, O., 2007. Miocene Central Paratethys stratigraphy - current status and future directions. Stratigraphy 4, 151–168.
Pinchuk, T.N., 2006. Biostratigraphy of the Cenozoic beds of Russia and adjacent regions based on foraminifers: Western Caucasus and Cisacucasia (Oligocene and Neogene). In: Practial Handbook on the microfauna of the USSR: Foraminifers of the Cenozoic. Nedra, Saint Petersburg, pp. 91–98.
Popescu, G., 1995. Contribution of the Sarmatian foraminifera of Romania. Rom. J. Paleontol. 76, 85–98.
Popescu, S.-M., 2006. Late Miocene and early Pliocene environments in the southwestern Black Sea region from high-resolution palynology of DSDP Site 380A (Leg 42B). Palaeogeogr. Palaeoclimatol. Palaeoecol. 238, 64–77. https://doi.org/10.1016/j.palaeo.2006.03.018.
Popov, S.V., Shcherba, I.G., Ilyina, L.B., Nevesskaya, L.A., Paramonova, N.P., Khondkarian, S.O., Magyar, I., 2006. Late Miocene to Pliocene palaeogeography of the Paratethys and its relation to the Mediterranean. Palaeogeogr. Palaeoclimatol. Palaeoecol. 238, 91–106. https://doi.org/10.1016/j.palaeo.2006.03.020.
Popov, S.V., Antipov, M.P., Zastrozhnov, A.S., Kurina, E.E., Pinchuk, T.N., 2010. Sea-level fluctuations on the northern shelf of the Eastern Paratethys in the Oligocene-Neogene. Stratigr. Geol. Correl. 18, 200–224. https://doi.org/10.1134/S0869593810020073.
Popov, S.V., Rostovtseva, Y.V., Fillippova, N.Y., Golovina, L.A., Radionova, E.P., Goncharova, I.A., Vernyhorova, Y.V., Dykan, N.I., Pinchuk, T.N., Iljina, L.B., Koromyslova, A.V., Kozyrenko, T.M., Nikolaeva, I.A., Viskova, L.A., 2016. Paleontology and stratigraphy of the Middle–Upper Miocene of the Taman Peninsula: part 1. Description of key sections and benthic fossil groups. Paleontol. J. 50, 1039–1206. https://doi.org/10.1134/S0031030116100014.
Posamentier, H.W., Walker, R.G., 2006. Facies models revisited. SEPM (Soc. Sed. Geol.) 84. https://doi.org/10.2110/pec.06.84.
Raaf, J.F.M., Boersma, J.R., Gelder, A., 1977. Wave-generated structures and sequences from a shallow marine succession, lower Carboniferous, County Cork, Ireland. Sedimentology 24, 451–483. https://doi.org/10.1111/j.1365-3091.1977.tb00134.x.
Radionova, E., Golovina, L., Filippova, N., Trubikhin, V., Popov, S., Goncharova, I., Vernigorova, Y., Pinchuk, T., 2012. Middle-upper miocene stratigraphy of the Taman

Peninsula, Eastern Paratethys. Open Geosci. 4, 925. https://doi.org/10.2478/s13533-011-0065-8.
Reading, H.G., 1996. Sedimentary environments: Processes, facies, and stratigraphy. In: Reading, H.G. (Ed.), Blackwell Science, Cambridge, Mass., Oxford, 3rd ed. .
Rögl, F., 1999. Mediterranean and Paratethys. Facts and hypotheses of an Oligocene to Miocene paleogeography (short overview). Geol. Carpath. 50, 339–349.
Roshka, V.K., 1973. The Meotian Mollusks of the South-Western Black Sea Region. Shtiintsa, Kishinev.
Rostovtseva, Y.V., Rybkina, A.I., 2017. The Messinian event in the Paratethys: Astronomical tuning of the Black Sea Pontian. Mar. Pet. Geol. 80, 321–332. https://doi.org/10.1016/j.marpetgeo.2016.12.005.
Roveri, M., Flecker, R., Krijgsman, W., Lofi, J., Lugli, S., Manzi, V., Sierro, F.J., Bertini, A., Camerlenghi, A., de Lange, G., Govers, R., Hilgen, F.J., Hübscher, C., Meijer, P.T., Stoica, M., 2014. The Messinian Salinity Crisis: past and future of a great challenge for marine sciences. Mar. Geol. 352, 25–58. https://doi.org/10.1016/j.margeo.2014.02.002.
Rybkina, A.I., Kern, A.K., Rostovtseva, Y.V., 2015. New evidence of the age of the lower Maeotian substage of the Eastern Paratethys based on astronomical cycles. Sediment. Geol. 330, 122–131. https://doi.org/10.1016/j.sedgeo.2015.10.003.
Sato, T., Chan, M.A., Ekdale, A.A., 2018. Trace Fossils and FLUVIAL-LACUSTRINE ICHNOFACIES of the Eocene Uinta and Duchesne River Formations, Northern Uinta Basin, Utah. giw. 5. pp. 209–226. https://doi.org/10.31711/giw.v5i0.27.
Scherer, C.M.S., Goldberg, K., Bardola, T., 2015. Facies architecture and sequence stratigraphy of an early post-rift fluvial succession, Aptian Barbalha Formation, Araripe Basin, northeastern Brazil. Sediment. Geol. 322, 43–62. https://doi.org/10.1016/j.sedgeo.2015.03.010.
Schmid, S.M., Bernoulli, D., Fügenschuh, B., Matenco, L., Schefer, S., Schuster, R., Tischler, M., Ustaszewski, K., 2008. The Alpine-Carpathian-Dinaridic orogenic system: correlation and evolution of tectonic units. Swiss J. Geosci. 101, 139–183. https://doi.org/10.1007/s00015-008-1247-3.
Schulz, H., Bechtel, A., Sachsenhofer, R., 2005. The birth of the Paratethys during the early Oligocene: from Tethys to an ancient Black Sea analogue? Glob. Planet. Chang. 49, 163–176. https://doi.org/10.1016/j.gloplacha.2005.07.001.
Seilacher, A., 2007. Trace Fossil Analysis. Springer, Berlin, London.
Simon, D., Palcu, D., Meijer, P., Krijgsman, W., 2019. The sensitivity of middle Miocene paleoenvironments to changing marine gateways in Central Europe. Geol 47, 35–38. https://doi.org/10.1130/G45698.1.
Snel, E., Mărunţeanu, M., Macaleţ, R., Meulenkamp, J.E., van Vugt, N., 2006. Late Miocene to early Pliocene chronostratigraphic framework for the Dacic Basin, Romania. Palaeogeogr. Palaeoclimatol. Palaeoecol. 238, 107–124. https://doi.org/10.1016/j.palaeo.2006.03.021.
Stevanovic, P.M., Iljina, L.B., 1982. Stratigrafija meotisa Vostochnoj Serbii i sosednikh regionov po molluskam. Bull. Acad. Serbe Sci. Arts, Cl. Sci. Nat. Math. Sci. Nat. 82, 105–136.
Stevanovic, P.M., Paramonova, N.P., 1983. Verhni Sarmat (Chersonslii regiojarus) Vostochnogo Paratetisa i ego stratigrafija v predkarpatskoj oblasti Serbii po molluskam. Bull. Acad. Serbe Sci. Arts, Cl. Sci. Nat. Math. Sci. Nat. 83, 55–100.
Stevanovic, P., Nevesskaya, L.A., Marinescu, F., Sokac, A., Jámbor, A. (Eds.), 1989. Neogen der Westlichen ("Zentralen") Paratethys, Pontien. JAZU & SANU, Zagreb-Beograd.
Stoica, M., Lazăr, I., Vasiliev, I., Krijgsman, W., 2007. Mollusc assemblages of the Pontian and Dacian deposits from the Topolog-Argeş area (southern Carpathian foredeep – Romania). Geobios 40, 391–405. https://doi.org/10.1016/j.geobios.2006.11.004.
Stoica, M., Lazăr, I., Krijgsman, W., Vasiliev, I., Jipa, D., Floroiu, A., 2013. Paleoenvironmental evolution of the East Carpathian foredeep during the late Miocene–early Pliocene (Dacian Basin; Romania). Glob. Planet. Chang. 103, 135–148. https://doi.org/10.1016/j.gloplacha.2012.04.004.
Stoica, M., Krijgsman, W., Fortuin, A., Gliozzi, E., 2016. Paratethyan ostracods in the Spanish Lago-Mare: more evidence for interbasinal exchange at high Mediterranean Sea level. Palaeogeogr. Palaeoclimatol. Palaeoecol. 441, 854–870. https://doi.org/10.1016/j.palaeo.2015.10.034.
Suess, E., 1866. Untersuchungen über den Charakter der österreichischen Tertiärbildungen II. Über die Bedeutung der sogenannten "brackischen Stufe" oder der "Cerithienschichten". Sitzungsberichte der Akademie der Wissenschaften, mathematisch-naturwissenschaftliche Klasse. 54. pp. 218–259.
Tamura, T., 2012. Beach ridges and prograded beach deposits as palaeoenvironment records. Earth Sci. Rev. 114, 279–297. https://doi.org/10.1016/j.earscirev.2012.06.004.
Tărăpoancă, M., Bertotti, G., Maţenco, L., Dinu, C., Cloetingh, S.A.P.L., 2003. Architecture of the Focşani Depression: a 13 km deep basin in the Carpathians bend zone (Romania). Tectonics 22https://doi.org/10.1029/2002TC001486. n/a-n/a.
Tari, G., Fallah, M., Kosi, W., Floodpage, J., Baur, J., Bati, Z., Sipahioğlu, N.Ö., 2015. Is the impact of the Messinian Salinity Crisis in the Black Sea comparable to that of the Mediterranean? Mar. Pet. Geol. 66, 135–148. https://doi.org/10.1016/j.marpetgeo.2015.03.021.
Tauxe, L., 2010. Essentials of Paleomagnetism. University of California Press, Berkeley.
Taviani, M., Remia, A., Esu, D., Sami, M., 2007. Messinian Lago-Mare mollusc fauna from the Gorgona Island slope, Tyrrhenian Sea. Geobios 40, 351–358. https://doi.org/10.1016/j.geobios.2007.02.001.
ter Borgh, M., Vasiliev, I., Stoica, M., Knežević, S., Matenco, L., Krijgsman, W., Rundić, L., Cloetingh, S., 2013. The isolation of the Pannonian basin (Central Paratethys): New constraints from magnetostratigraphy and biostratigraphy. Glob. Planet. Chang. 103, 99–118. https://doi.org/10.1016/j.gloplacha.2012.10.001.
ter Borgh, M., Stoica, M., Donselaar, M.E., Matenco, L., Krijgsman, W., 2014. Miocene connectivity between the Central and Eastern Paratethys: Constraints from the western Dacian Basin. Palaeogeogr. Palaeoclimatol. Palaeoecol. 412, 45–67. https://doi.org/10.1016/j.palaeo.2014.07.016.
Trubikhin, V.M., 1989. Paleomagnetic data from the Pontian. In: Stevanovic, P., Nevesskaya, L.A., Marinescu, F., Sokac, A., Jámbor, A. (Eds.), Neogen der Westlichen ("Zentralen") Paratethys, Pontien. JAZU & SANU, Zagreb-Beograd, pp. 76–79.
Tucker, M.E., 2012. Sedimentary rocks in the field: a practical guide. Environ. Eng. Geosci. 18, 401–402. https://doi.org/10.2113/gseegeosci.18.4.401-b.
Tugolesov, D.A., Gorshkov, A.S., Meisner, L.B., Solov'ev, V.V., Khakhalev, E.M., 1985. Tectonic of the of the Mezo-Ceinozoic Deposits in the Black Sea Depression (In Russian). Nedra, Moscow.
van Baak, C.G.C., Mandic, O., Lazar, I., Stoica, M., Krijgsman, W., 2015. The Slanicul de Buzau section, a unit stratotype for the Romanian stage of the Dacian Basin (Plio-Pleistocene, Eastern Paratethys). Palaeogeogr. Palaeoclimatol. Palaeoecol. 440, 594–613. https://doi.org/10.1016/j.palaeo.2015.09.022.
van Baak, C.G.C., Stoica, M., Grothe, A., Aliyeva, E., Krijgsman, W., 2016. Mediterranean-Paratethys connectivity during the Messinian salinity crisis: the Pontian of Azerbaijan. Glob. Planet. Chang. 141, 63–81. https://doi.org/10.1016/j.gloplacha.2016.04.005.
van Baak, C.G.C., Krijgsman, W., Magyar, I., Sztanó, O., Golovina, L.A., Grothe, A., Hoyle, T.M., Mandic, O., Patina, I.S., Popov, S.V., Radionova, E.P., Stoica, M., Vasiliev, I., 2017. Paratethys response to the Messinian salinity crisis. Earth Sci. Rev. 172, 193–223. https://doi.org/10.1016/j.earscirev.2017.07.015.
van Cappelle, M., Stukins, S., Hampson, G.J., Johnson, H.D., 2016. Fluvial to tidal transition in proximal, mixed tide-influenced and wave-influenced deltaic deposits: cretaceous lower Sego Sandstone, Utah, USA. Sedimentology 63, 1333–1361. https://doi.org/10.1111/sed.12267.
van der Kolk, D.A., Flaig, P.P., Hasiotis, S.T., 2015. Paleoenvironmental reconstruction of a late cretaceous, Muddy, River-dominated polar deltaic system: schrader bluff—prince creek formation transition, Shivugak Bluffs, North Slope of Alaska, U.S.A. J. Sediment. Res. 85, 903–936. https://doi.org/10.2110/jsr.2015.58.
Vasiliev, I., Krijgsman, W., Langereis, C.G., Panaiotu, C.E., Maţenco, L., Bertotti, G., 2004. Towards an astrochronological framework for the eastern Paratethys Mio–Pliocene sedimentary sequences of the Focşani basin (Romania). Earth Planet. Sci. Lett. 227, 231–247. https://doi.org/10.1016/j.epsl.2004.09.012.
Vasiliev, I., Krijgsman, W., Stoica, M., Langereis, C.G., 2005. Mio-Pliocene magnetostratigraphy in the southern Carpathian foredeep and Mediterranean-Paratethys correlations. Terra Nova 17, 376–384. https://doi.org/10.1111/j.1365-3121.2005.00624.x.
Vasiliev, I., Franke, C., Meeldijk, J.D., Dekkers, M.J., Langereis, C.G., Krijgsman, W., 2008. Putative greigite magnetofossils from the Pliocene epoch. Nat. Geosci. 1, 782–786. https://doi.org/10.1038/ngeo335.
Vasiliev, I., Maţenco, L., Krijgsman, W., 2009. The syn- and post-collisional evolution of the Romanian Carpathian foredeep: New constraints from anisotropy of magnetic susceptibility and paleostress analyses. Tectonophysics 473, 457–465. https://doi.org/10.1016/j.tecto.2009.04.002.
Vasiliev, I., de Leeuw, A., Filipescu, S., Krijgsman, W., Kuiper, K., Stoica, M., Briceag, A., 2010. The age of the Sarmatian–Pannonian transition in the Transylvanian Basin (Central Paratethys). Palaeogeogr. Palaeoclimatol. Palaeoecol. 297, 54–69. https://doi.org/10.1016/j.palaeo.2010.07.015.
Vasiliev, I., Reichart, G.-J., Grothe, A., Sinninghe Damsté, J.S., Krijgsman, W., Sangiorgi, F., Weijers, J.W.H., van Roij, L., 2015. Recurrent phases of drought in the upper Miocene of the Black Sea region. Palaeogeogr. Palaeoclimatol. Palaeoecol. 423, 18–31. https://doi.org/10.1016/j.palaeo.2015.01.020.
Vereshchagin, V.N. (Ed.), 1982. Stratigraphic Dictionary of the USSR: Paleogene, Neogene, Quternary System. Nedra, Leningrad.
Vincent, S.J., Davies, C.E., Richards, K., Aliyeva, E., 2010. Contrasting Pliocene fluvial depositional systems within the rapidly subsiding South Caspian Basin; a case study of the palaeo-Volga and palaeo-Kura river systems in the Surakhany Suite, Upper Productive Series, onshore Azerbaijan. Mar. Pet. Geol. 27, 2079–2106. https://doi.org/10.1016/j.marpetgeo.2010.09.007.
Went, D.J., Hamilton, R.V., Platt, N.H., Underhill, J.R., 2013. Role of forced regression in controlling Brent Group reservoir architecture and prospectivity in the northern North Sea. Pet. Geosci. 19, 307–328. https://doi.org/10.1144/petgeo2013-028.
Wenz, W., 1942. Die Mollusken des Pliozäns der rumänischen Erdöl-Gebiete als Leitversteinerungen für die Aufschluss-Abeiten. Senckenbergiana 24, 1–293.
WoRMS Editorial Board, 2020. World Register of Marine Species. https://doi.org/10.14284/170. https://www.marinespecies.org Accessed 2019-07-18.
Yoshida, S., 2000. Sequence and facies architecture of the upper Blackhawk Formation and the lower Castlegate Sandstone (Upper cretaceous), Book Cliffs, Utah, USA. Sediment. Geol. 136, 239–276. https://doi.org/10.1016/S0037-0738(00)00104-4.
Zhu, Y., Bhattacharya, J.P., Li, W., Lapen, T.J., Jicha, B.R., Singer, B.S., 2012. Milankovitch-scale sequence stratigraphy and stepped forced regressions of the turonian ferron notom deltaic complex, South-Central Utah, U.S.A. J. Sediment. Res. 82, 723–746. https://doi.org/10.2110/jsr.2012.63.